
Article:
Metilli, L, Lazidis, A, Francis, M et al. (3 more authors) (2021) The Effect of Crystallization Conditions on the Structural Properties of Oleofoams Made of Cocoa Butter Crystals and High Oleic Sunflower Oil. Crystal Growth and Design, 21 (3). pp. 1562-1575. ISSN 1528-7483

https://doi.org/10.1021/acs.cgd.0c01361

Effect of crystallization conditions on the structural properties of oleofoams made of cocoa butter crystals and high oleic sunflower oil

Lorenzo Metilli[1], *Aris Lazidis*[2], *Mathew Francis* [1], *Stephanie Marty-Terrade*[2], *Joydeep Ray*[3], *Elena Simone*[1]*

[1] School of Food Science and Nutrition, Food Colloids and Bioprocessing group, University of Leeds, Woodhouse Lane, Leeds LS2 9JT, UK

[2] Nestlé Product Technology Centre, Haxby Road, York YO31 8TA, UK

[3] Nestlé Research, Vers-chez-les-Blanc, 1000 Lausanne 26, Switzerland

***Corresponding author:** e.simone@leeds.ac.uk

Keywords: cocoa butter, oleogel, oleofoam, crystallization

ABSTRACT

Edible air-in-oil systems, also referred to as oleofoams, constitute a novel promising material for healthier, low-calorie fat replacers in confectionary products. Oleofoams can be formed by whipping oleogels, which are dispersions of fat crystals in an oil phase. Understanding how the properties of the fat crystals (*i.e.* size, shape, polymorphism) contained in oleogels affect the microstructure and stability of oleofoams is essential for both the efficient design and manufacture of novel food products. In this work, cocoa butter – one of the main fat phases present in confectionary productions, which is responsible for pleasant texture and mouthfeel properties – was mixed with high oleic sunflower oil and crystallized to obtain an oleogel. This was subsequently whipped to yield a stable, highly aerated oleofoam. The effect of the crystallization conditions (oleogel composition and cooling rate) on the properties of the oleogels and related oleofoams was investigated with a multi-technique characterization approach, featuring polarized light microscopy, cryogenic scanning electron microscopy, X-Ray diffraction, differential scanning calorimetry and oscillatory rheology. Oleogel crystallization was performed in a lab-scale vessel, and was monitored using light turbidimetry as an *in* situ technique. Results showed that the concentration of cocoa butter in sunflower oil was the parameter that affected most strongly the foamability and rheology of oleofoam samples. The size and shape of cocoa butter crystals within the oleogel was found to have a less significant effect, since crystals were broken or partially melted during the aeration process. Oleofoams whipped from oleogels containing 15% w/w and 22% w/w cocoa butter displayed an overrun of 200% – corresponding to a calorific density reduction to one-third – and an increase in both the elastic and viscous moduli compared to their oleogel precursor. This was explained by a structuring effect caused by the aeration process, where cocoa butter β(V) crystal nanoplatelets (CNPs) in the oleogel rearranged to stabilize

the air bubbles *via* a Pickering mechanism. Oleofoams prepared from 30% w/w cocoa butter oleogels, on the other hand, incorporated less air (overrun between 150% and 180%) and displayed a similar viscoelastic profile to their un-whipped precursors, potentially due to air incorporation being limited by the relatively high elastic modulus of the parent oleogels. Nevertheless, the calorific density of these samples was reduced by a factor of 1.6 to 2.5 compared to their full-fat analogues.

INTRODUCTION

The prevalence of overweight and obese population in several countries has been described as a global pandemic, causing in 2015 an estimated 4.0 million deaths, along with 120 million people living with disabilities[1]. Several factors promote obesity and related health conditions in individuals, but excessive dietary caloric intake is the predominant cause[2]. Edible lipids (such as fats and oils) constitute the most energy-dense macronutrient, and their effects on health have been studied since the 1950s, with a particular focus on saturated fats. The role of saturated fats in directly promoting obesity has still not fully been proven[3], but dietary guidelines issued by the Food and Agriculture Organization (FAO) and the European Food Safety Authority (EFSA) advised the reduction of saturated fats to 10% of the total daily caloric intake, and their replacement with polyunsaturated fatty acids (PUFAs), commonly found in oils[4,5]. Therefore, food research has recently focused on reformulating food products with a reduced level of saturated fats, while maintaining desirable sensory attributes[6]. Nevertheless, saturated fats have a critical role in determining desirable physiochemical and sensorial attributes in foods, hence making their replacement or reduction challenging. Confectionary products are an example of food rich in

saturated fats[7,8]. The main ingredient of chocolate and chocolate fillings, cocoa butter, contains around 60% w/w saturated fats, mainly from stearic acid. Cocoa butter beneficially affects the rheology of such products, their melting behaviour and flavour release[7]. Reducing this type of fats in food products is not only driven by health concerns, but is further underscored by environmental and economic issues related to sustainable cocoa butter production[9,10].

Oleogelation of edible oils has been proposed as a viable replacement of saturated fats in food formulation, as it results in similar rheological and sensorial properties, but lower saturated fat content. Oleogelation is the process of adding an edible oil (up to 90% w/w) to gelator molecules that are able to convert the liquid oil into a gel, with solid-like properties. This is achieved through the formation of a three-dimensional, supramolecular network of either molecules or crystals that entraps the oil phase. Commonly used gelators are high-melting triacylglycerides (TAGs), di-glycerides (DAGs) or monoglycerides (MAGs), fatty acids and fatty alcohols, as well as edible waxes, ethyl cellulose or native phytosterols[11]. Oleogels have been used to replace saturated fat in foods, such as baking shortenings, spreads and margarines[12,13]. Additionally, oleogels have been used to reformulate confectionery fillings and chocolate pastes with reduced saturated fat and resistance to oil migration[14–16].

While oleogelation improves significantly the nutritional profile of full-fat products through the reduction in saturated fats, it still involves the use of large amounts of edible oils in their formulation, retaining a similar calorific content to solid fat. Incorporating gas bubbles in oleogels is a possible solution to decrease their calorific content while maintaining appealing rheological and sensory (*e.g.* creaminess) properties[17]. Moreover, aerated foods induce satiety independently of their calorific content[18], and deliver a comparable mouth coating to their non-aerated analogues, stimulating the oral mechanoreceptors in a similar fashion[19]. Stable air bubbles can also be

incorporated in oleogels and stabilized *via* a Pickering mechanism, whereby solid fat crystals are adsorbed at the air/oleogel interface preventing phase separation and coalescence. Aerated oleogels, also called oleofoams, have recently gained attention due to their potential to reformulate food products with lower calorific density[20]. In fact, the use of oleofoams for reducing fat content and calorific density in confectionery has been reported in at least two patents[21,22].

Typically, oleofoams are produced by adding a high-melting fat (*e.g.* a food-grade monoglyceride) to a vegetable oil in the molten state, followed by cooling to yield a dispersion of fat crystals. Subsequently, the material is whipped to entrain air bubbles under shear, which are coated by the fat crystals to produce a stable foam. Hence, controlling the crystal size dispersity by fine-tuning the crystallization process parameters is a fundamental aspect of oleofoam production. Other methods of aeration involved the injection of inert gases in the continuous phase, or application of vacuum followed by expansion of small gas bubbles in the continuous phase[23].

Given the central role of crystals in the formation of oil-base foams, their concentration in the oil, their size, shape and polymorphism are pivotal to determining the microstructure, foamability (*i.e.* the amount of incorporated air), the viscoelasticity and stability of oleofoams[24]. TAGs, one of the main chemical species in fats and oils, also exhibit complex polymorphism. The main crystal polymorphs are, in increasing order of thermodynamic stability, α (hexagonal subcell), β' (orthorhombic subcell) and β (triclinic subcell)[25].

Oleofoam aeration can only be achieved in a specific range of crystalline concentrations. Below the lower limit there is an insufficient quantity of fat crystals to stabilize the foam, whereas an excessive amount of solids results in a very firm oleogel, which is difficult to aerate[26–28]. Those limits are, however, system-dependent and also affected by the aeration equipment used to produce oleofoams [24].

Micron-sized needle or platelet-shaped crystals were found to be most effective at stabilizing air bubbles, as opposed to larger or aggregated crystals. Mishima et al. (2016) prepared oleogels from TAGs crystals (fully hydrogenated rapeseed oil rich in behenic acid, FHR-B) in salad oil (a mixture of soybean and rapeseed oil) using different tempering protocols. The study found that oleogels containing small (2-6 μm in length) crystals were able to incorporate more air in less whipping time, compared to oleogels containing larger crystals (10-30 μm in length)[29]. In some cases, oleogels containing large crystals of monostearin and native phytosterol (NPS) obtained with slow cooling rates could not be aerated at all, as reported by Truong et al. (2019)[30].

Lack of control over the polymorphic form nucleated during crystallization resulted in poor foamability, as reported by Mishima et al. (2016) for the above-mentioned salad oil and FHR – B system. The authors showed that oleogels containing tempered β crystals were able to produce highly aerated foams, whereas untempered β' oleogels barely incorporated any air[29]. Heymans et al. (2018) investigated further the effect of polymorphism on the foamability of oleogels[31]. In this work, five tempering protocols were used to prepare oleogels with sub-α crystals (SAC), partially and fully crystallized α crystals (PAC and AC, respectively), melt-mediated β crystals (MMACS) and solid-state transformed β crystals (ACS) from a commercial monoglyceride and sunflower oil. AC and MMACS oleogels produced oleofoams with similar overruns, PAC oleogels incorporated slightly more air but were unstable and subject to oil drainage in storage, while SAC oleogels could not be aerated at all. However, it is not clear from the study whether the latter polymorph melted during aeration or if it was not surface-active. Control over crystallization is critical to ensure oleogel precursors with suitable crystalline properties for aeration. In industrial settings, crystallization is a complex process, affected by several factors, such as shearing, thermal fluctuations and presence of impurities[32,33].

Vegetable oils could be aerated in absence of added high-melting fat species, as recently demonstrated by Liu & Binks (2021)[34]. The authors prepared oleogels by cooling peanut oil and olive oil down to –20°C in order to crystallize the unsaturated TAGs present in the oil. Oleofoams were produced with modest overrun values (40% for peanut oil, 110% for olive oil oleogels) while maintaining the aeration temperature below 0°C. In a previous publication, Binks & Marinopoulos (2017) demonstrated also the ability of natural fats to produce oleofoams, including cocoa butter[35].

However, the properties of cocoa butter crystals and how they relate to the final oleofoam microstructure were not considered in such work. Cocoa butter has a complex crystallization behaviour and it is a key ingredient in many confectionary products, including chocolate fillings. Therefore, obtaining a better understanding of how the properties of cocoa butter crystals affect the stability and microstructure of oleofoams is essential for the design of novel confectionary products and manufacturing processes. In particular, this work aims to investigate the effect of crystallization conditions on the properties of oleogels as well as on the microstructure and stability of the derived oleofoams. The crystallization of cocoa butter-based oleogels was carried out in a laboratory-scale vessel and monitored *in* situ with light turbidimetry. Cocoa butter was mixed with high oleic sunflower oil, which displays high resistance to oxidation[36], in order to reduce the total amount of saturated fats of the system compared to pure cocoa butter.

Three cooling rates and three suitable concentrations of cocoa butter in sunflower oil were chosen for preparing the oleogel precursor. These concentrations were selected to ensure the presence of a sufficient amount of stabilizing crystals without yielding oleogels that were too firm to aerate. The effects of the size, morphology and polymorphism of cocoa butter crystals on the microstructure, rheology and foamability of oleogels and related oleofoams was then investigated with a multi-technique approach. This included polarized light microscopy (PLM), cryogenic

scanning electron microscopy (CryoSEM) for the crystal morphology, X-Ray diffraction (XRD) for crystal polymorphism, differential scanning calorimetry (DSC) for the melting properties and oscillatory rheology for the viscoelasticity.

EXPERIMENTAL SECTION

Materials

Refined, bleached and deodorised cocoa butter (CB) and high-oleic sunflower oil (HOSO) were kindly provided by Nestlé PTC (York, UK) and used without any further purification. Typical fatty acid composition by weight of HOSO is 86 % oleic acid, 5% stearic acid, 3% linoleic acid, 3 % palmitic acid, 1.5% behenic acid and 0.7% arachidic acid [37]. CB normally contains by weight about 26 % palmitic acid, 36% stearic acid, 34% oleic acid, 2.7% linoleic and 0.9% of arachidic acid [38].

CB was melted at 65°C for at least 30 minutes, using a stirring hot plate. It was then mixed with HOSO in three different concentrations (15, 22 and 30% of CB by weight). Samples with % CB w/w below 15% were also tested but they melted rapidly and produced oleofoams with significant oil drainage; hence, they were not investigated further. Throughout this paper, oleogel and oleofoam samples were named based on their CB concentration and the cooling rate used during crystallization: F for fast cooling (0.75°C/min), M for medium cooling (0.25°C/min) and S for slow cooling (0.10°C/min). Cocoa butter seeds in the β(V) polymorph were purchased from Callebaut (Zurich, Switzerland) and used as reference for the crystalline form in oleogel and oleofoam samples in this paper.

Synchrotron Radiation X-Ray Diffraction (SR-XRD)

The crystallization behaviour of cocoa butter in sunflower oil in quiescent conditions was investigated with synchrotron radiation X-Ray diffraction (SR-XRD, $\lambda = 0.69$ Å) using beamline I22 at Diamond Light Source (DLS, Didcot, UK). The sample-to-detector distance (SDD) was set to 8.732 m and the 2D diffraction patterns were recorded on a Pilatus 2M detector (Dectris Ltd, Switzerland). Disposable polycarbonate capillaries (diameter 2 mm) were filled with mixtures of melted CB and HOSO in different weight ratios (15%, 22%, 32% w/w) and loaded into a temperature-controlled multi-capillary rack, controlled with an external water circulator (Lauda, Germany). The temperature was initially set to 65°C for 5 minutes, followed by stepwise cooling to 20, 15 10 and 7 °C at approximately -1 °C/min. Each temperature was maintained for 5 minutes prior to the measurement, after that the diffraction pattern of each sample was collected. The exposure time was set to 1.0 seconds. An empty polycarbonate capillary was used for background scattering subtraction. Diffraction images were analysed using the DAWN software and following the procedure outlined by Filik et al. (2017)[39]. The signal of the melted samples was subtracted using MATLAB 2020a (MathWorks, USA). A detailed explanation of the subtraction procedure used is provided in the Supporting Information 1.

Oleogel Crystallization and Aeration

A total mass of 450g of molten cocoa butter and sunflower oil mixtures at the three concentrations of 15, 22 and 30% CB w/w were poured into a custom-made steel jacketed vessel (capacity *ca.* 2 L, diameter 25 cm) connected to a Huber Ministat 250 thermostat (Huber, Germany) filled with mineral oil as heating/cooling medium. Samples were stirred continuously at 200 rpm with a DLH

Overhead Stirrer (VELP Scientifica, Italy), equipped with a 4 pitched-blade impeller (4 cm diameter). A Pt-100 temperature probe was placed inside the vessel to measure the temperature of the mixture during crystallization. A schematic of the crystallization setup used for the experiments is shown in Figure 1.

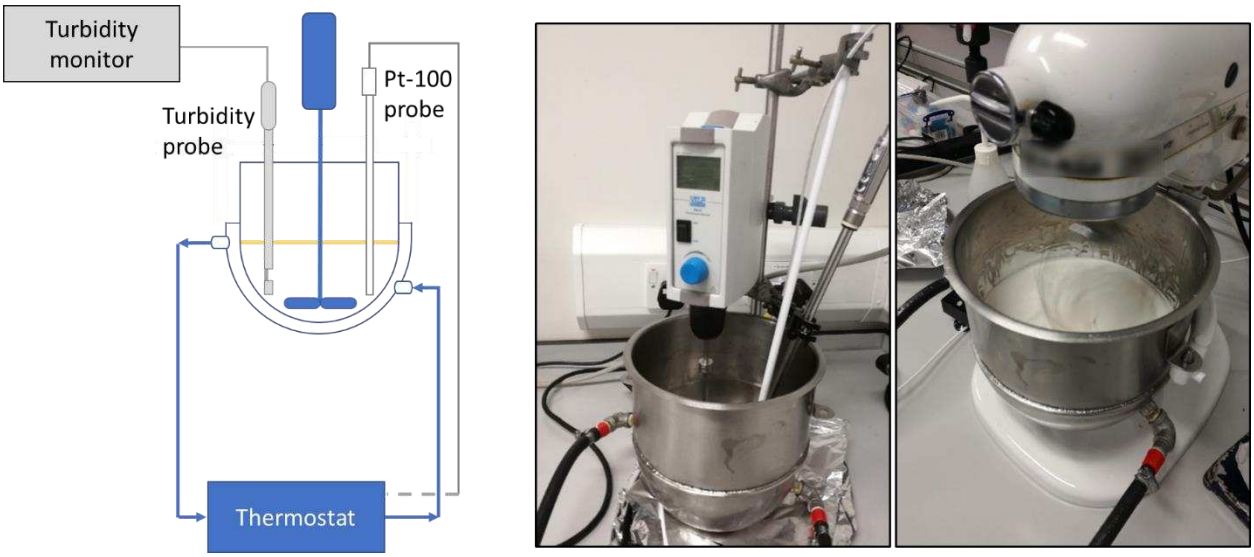

Figure 1. Schematics and photographs of the rig used for the crystallization and aeration experiments.

The initial thermal profile for the cocoa butter crystallization and the formation of the oleogels was the same for all experiments performed and it was set as following: after being molten at 65 °C for 30 minutes, the mixture was transferred in the crystallization vessel and allowed to equilibrate at 65 °C for further 5 minutes, and then cooled from 65 °C to 37 °C at –1 °C/min cooling rate. After that, each oleogel mixture (15, 22 and 30% CB w/w) was cooled from 37 °C to 0 °C with a nominal rate of –0.75, –0.25 or –0.10 °C/min (C_r). Each experiment was repeated in triplicates. The crystallization process was monitored with a Control 4000 turbidity meter (Optek, Germany) fitted with an ASD12-N Absorption Probe. Upon the onset of crystallization, the transmittance signal

started to drop due to increased turbidity in the sample. Once crystallized, the sample was left to equilibrate at the final temperature until a stable absorbance reading was seen. Light absorbance is approximately correlated to the amount of solid particles scattering the incoming light[40]; hence, a stable absorbance reading was interpreted as the reach of crystallization equilibrium at the final temperature. The oleogels thus obtained were manually mixed to obtain a homogeneous sample and their density measured volumetrically by weighting a measuring cup of a fixed volume of 30 mL. Density measurements were conducted in triplicates for each oleofoam produced. The effective cooling rates were calculated by linearly fitting the measured temperature of the samples between 37 °C and their crystallization temperatures (T_{Cr}).

The crystallized oleogel samples were then aerated using a Heavy Duty model 5KPM50 planetary mixer (Kitchenaid, USA) machine equipped with a wire beater. The temperature of the jacketed vessel was maintained at 0 °C during the aeration process. The temperature of the oleofoam was monitored during whipping using a portable kitchen thermometer, measuring the sample in five different points inside the aeration vessel. The whipping speed was set to 180 rpm for all experiments. Oleogels were whipped in cycles of 5 minutes with 10 minutes rest, for a total aeration time of 30 minutes. Solid un-whipped oleogel on the vessel walls was reintroduced with a spatula as necessary. During the resting stage the overrun of the oleofoams was calculated by measuring the weight of the measuring cup of known volume filled with the aerated sample. Measurements were done in triplicates. The overrun was calculated according to Equation 1[31] and then plotted as a function of whipping time:

$$OR(\%) = 100 \times \frac{\left(w_{oleogel} - w_{foam}\right)}{w_{foam}} \qquad \text{Eq. 1}$$

Where $w_{oleogel}$ is the weight of a fixed volume of oleogel, while w_{foam} is the weight of the same volume of oleofoam. Oleofoam and oleogel samples were collected at each aeration step and stored in a temperature-controlled cabinet at 20 °C for three months.

Polarized Light Microscopy

Cocoa butter crystals formed in sunflower oil were observed with a Leitz Dialux 22 polarized microscope (Leica, Germany) in both oleogel and oleofoam samples. A small amount of sample (point of a spatula) was placed on a glass microscope slide and gently covered with a glass cover slip. Digital images of each samples were acquired with a Canon DLSR camera at 10x and 40x magnification, and processed with ImageJ 1.52a (National Institute of Health, USA). An estimate of the average crystals' diameter was calculated by measuring the size of around 100 crystals from 5 different images collected for each sample.

Cryogenic Scanning Electron Microscopy

The microstructure of oleogel and oleofoam samples was investigated by using a Helios G4 CX DualBeam scanning electron microscope (FEI, USA), coupled with a PP3010T Cryo-FIG/SEM preparation system (Quorum Technologies, UK). A small amount of the sample was placed in a pre-cooled rivet holder and quickly transferred into a container filled with liquid nitrogen. The rivet containing the sample was then inserted in the preparation chamber and kept at –145 °C under vacuum ($<10^{-7}$ mbar). The frozen sample was then fractured in the middle of the rivet using a cooled sharp knife and sublimed at –90 °C to avoid any frost depositing on the surface, then cooled

again to –145 °C. In order to avoid charge build-up while imaging, the sample surface was sputtered with iridium (10 mA for 30 s). The sample was then transferred inside the microscope chamber and imaged using a 2 kV accelerating voltage and 0.10 nA beam current. The diameter of the air bubbles and the size of the crystals was evaluated using ImageJ 1.52a (National Institute of Health, USA).

Benchtop X-Ray Diffraction

Cocoa butter polymorphism in oleogels and oleofoams prepared in the laboratory-scale vessel was determined by X-Ray diffraction experiments, with a SAXSpace instrument (Anton Paar GmbH, Austria) equipped with a Cu-anode operating at 40 kV and 50 mA (λ=0.154 nm). The temperature inside the sample chamber was regulated with a TCStage 150 Peltier element (Anton Paar, Austria) and set to 20 °C for all experiments, to resemble the oleogel and oleofoam storage temperature. Samples were loaded into a Paste Cell equipped with X-Ray transparent Kapton windows. The 1D diffraction patters were recorded with a Mythen X-ray detector (Dectris Ltd, Switzerland). Small-angle and wide-angle measurements were obtained by changing the sample to detector distance (SDD) to 317 or 130 mm, respectively. The acquisition time used was 200 s for all experiments. Three measurements for each sample were collected.

Differential Scanning Calorimetry

The melting temperature (T_m) of the produced oleogels and oleofoams was determined by differential scanning calorimetry (DSC) using a Perkin Elmer 8000 calorimeter (Perkin Elmer,

USA) and a TA 8000 (TA Instruments, USA). The samples were melted from 10 °C to 65 °C at a heating rate of 5 °C/min. DSC measurements were carried out in triplicates, and the average endothermic peak maximum temperature (T_m) was calculated.

Oscillatory Rheology

Amplitude sweeps of oleogel and oleofoam samples were carried out on an MCR 302 stress-controlled rheometer in order to measure sample elastic and viscous moduli. A 25mm parallel plate was used for all experiments, with a sample gap of 1.0 mm. Amplitude sweeps at a fixed frequency of 1 Hz were performed from 0.001% to 10% strain. The temperature was maintained constant with a Peltier hood connected to a F25-HE water circulator (Julabo, Seelbach, Germany) at 20°C. Samples were measured 24 hours after they were crystallized or aerated. Each sample was measured in triplicates. Data analysis was carried out with the Rheocompass version 1.21 (Anton Paar GmbH, Austria). The elastic modulus in the linear viscoelastic regime (G'_{LVER}) was calculated by averaging the G' values between 0.001% and 0.01% strain, where both viscous and elastic moduli were observed to be independent of the applied strain[28]. The flow point (τ_f) was calculated as the crossing point of the elastic and viscous curve.

Oil Drainage and Stability Test

In order to assess the destabilization of oleofoam samples due to oil drainage, 50 mL of oleofoam samples from the final whipping cycle were transferred into graduated cylinders (2 cm diameter)

and left in temperature-controlled storage at 20°C. Samples were visually inspected every 2 weeks for 3 months. The volume of drained oil was measured volumetrically over time.

RESULTS AND DISCUSSION

Crystallization behaviour of CB/HOSO mixtures in capillaries

The effect of CB concentration on the crystallization behaviour of CB/HOSO mixtures was investigated first in quiescent conditions (small volume and absence of shear) with SR-XRD. The aim of this set of experiments was to get a basic understanding of the crystallization behaviour of CB/HOSO mixtures and to relate these results with the behaviour of the same oleogels in the lab-scale crystallization rig, under the effect of shear and using a larger volume.

Figure 2 shows the diffraction patterns of CB/HOSO mixtures cooled down to different temperatures from the melt. In order to highlight the presence of peaks from the cocoa butter crystals, the WAXS patterns in Figure 2 were obtained by subtracting the signal of the molten mixture at 20 °C from the respective signals of the crystallizing mixtures at 15, 10 and 7 °C.

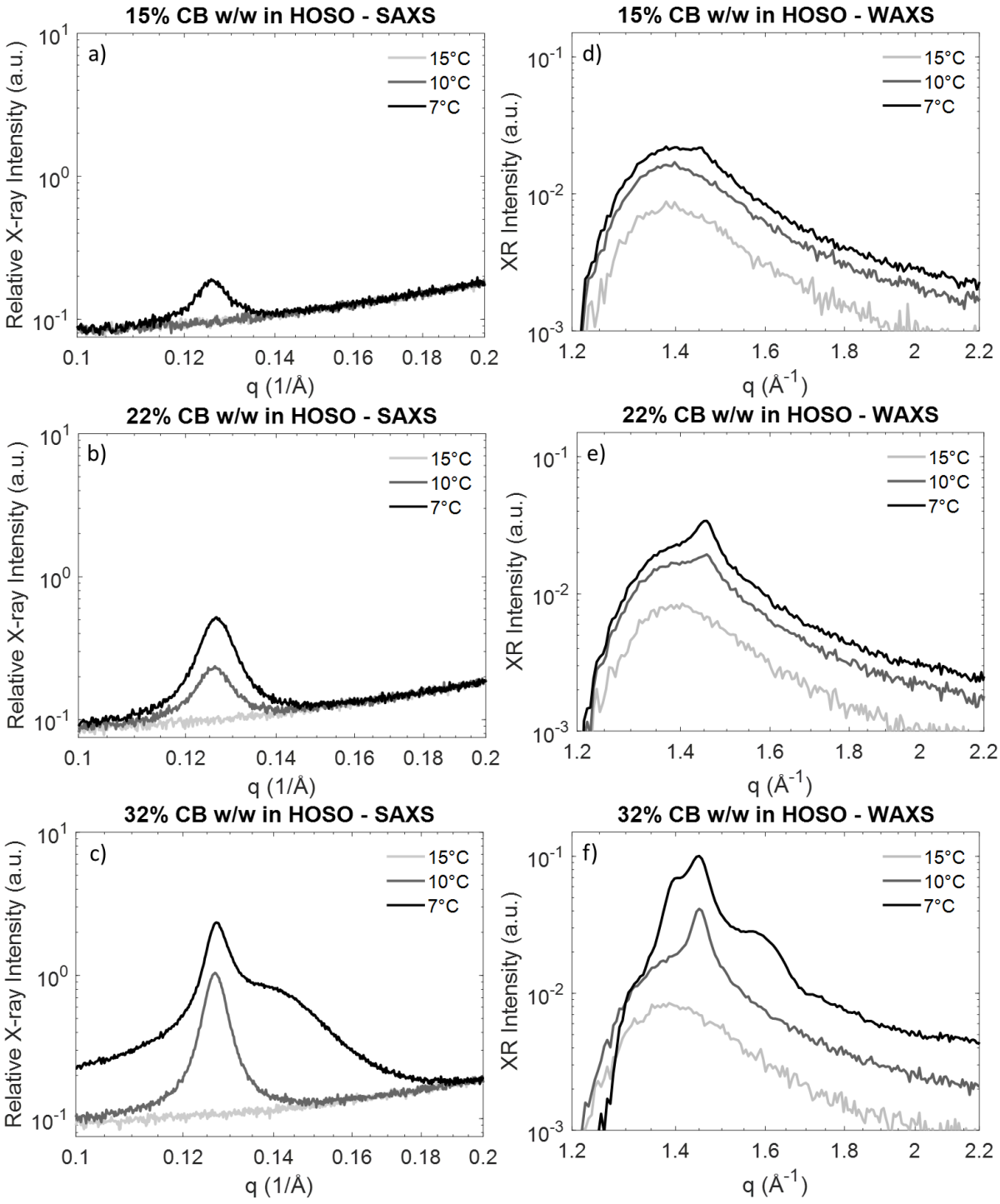

310

311 **Figure 2**. Synchrotron X-Ray diffraction patterns for the crystallization of CB/HOSO mixtures in

312 capillaries during cooling. Small angle region from a) to c) (without melt subtraction), wide angle

313 region from d) to f) (with melt subtraction).

The molten phase generates a broad scattering peak between q = 0.6 $Å^{-1}$ and q = 2.3 $Å^{-1}$ in the wide-angle region. Sections of this region were used to determine the baseline for each WAXS pattern. A detailed description of the baseline determination and subtraction procedure is provided in Supporting Information 1. Unfortunately, the position of the broad signal of the molten CB shifted towards higher q values with decreasing temperatures making. This is why it is still partly visible in some diffraction pattern even after baseline subtraction; this artefact is likely affecting the position of the WAXS peaks.

In the CB/HOSO mixture with 15% CB w/w crystals were detected only at 7 °C, with the appearance of a peak at q = 0.126 $Å^{-1}$ in the small angle scattering region (Figure 2a) and a weak intensity peak at around q = 1.46 $Å^{-1}$ (Figure 2d). These peaks corresponds to long and short spacing values of 49.9 and around 4.3 Å respectively; and they can be both associated to the formation of the 2L lamellar structure of the metastable α form of cocoa butter[41]. At higher concentrations of cocoa butter (22 and 32% w/w) crystalline material is detected also at 10°C. This is because increasing the concentration of CB generates an increase in the melting temperature of CB/HOSO mixtures, determining a higher level of undercooling at a given temperature, thus higher driving force for crystal nucleation and growth. As shown in Figure 2b and 2e, the observed peaks for the sample at 22% w/w CB are in the same position of the ones observed for the 15% w/w CB sample (q = 0.127 $Å^{-1}$ and 1.46 $Å^{-1}$), indicating the presence of the α polymorph of cocoa butter also for this oleogel. The same polymorphic structure can be observed in the 32% w/w CB oleogel at both 10 and 7°C (Figure 2c and 2f). As shown in Figure 2c and 2f, at 7°C this last oleogel sample presents an additional peak in the small angle region at q = 0.137 $Å^{-1}$ (long spacing equivalent to 45.9 Å), and extra two peaks in the wide-angle region at around q = 1.39 $Å^{-1}$ (d = 4.51 Å) and q = 1.59 $Å^{-1}$ (d = 3.96 Å). The presence of these peaks indicates the formation of the

more compact 2L lamellar structure of the β'(IV) polymorph, which co-exist with the α polymorph at 7 °C[38,39]. The observed deviations in the position of the WAXS peak from the reported values for cocoa butter crystals in Loisel et al. (1998)[41] might be due to the presence of mixed crystals, which may include TAGs from the liquid HOSO in their lattice. This observation was previously reported for blends of vegetable oils and cocoa butter content below 30% w/w in Perez-Martinez et al. (2005)[42].

The 32% w/w CB sample is the only one that formed the β'(IV) crystal structure during the experiment. This CB/HOSO mixture has the highest melting point and, at 7 °C, it is the most undercooled in respect to the β'(IV) form. This can explain why this polymorph is only observed for this oleogel. Finally, it is worth noticing that the intensity of the α form peaks at the same temperature increases with increasing concentration of CB in HOSO due to the higher amount of solid material formed.

Laboratory scale crystallization and offline characterization of CB/HOSO oleogels

Figure 3 shows the temperature (jacket and sample) and turbidity signals (transmittance and absorbance) during the crystallization of a selected CB/HOSO oleogel in the lab-scale setup. As the mixture was stirred and cooled down to its nucleation temperature, its visual appearance changed from a transparent liquid to a turbid, viscous gel. Light turbidimetry was used to detect the onset of crystallization, which was associated to a steep decrease in transmittance, as well as to determine end-of-crystallization, at which a constant absorbance value was reached.

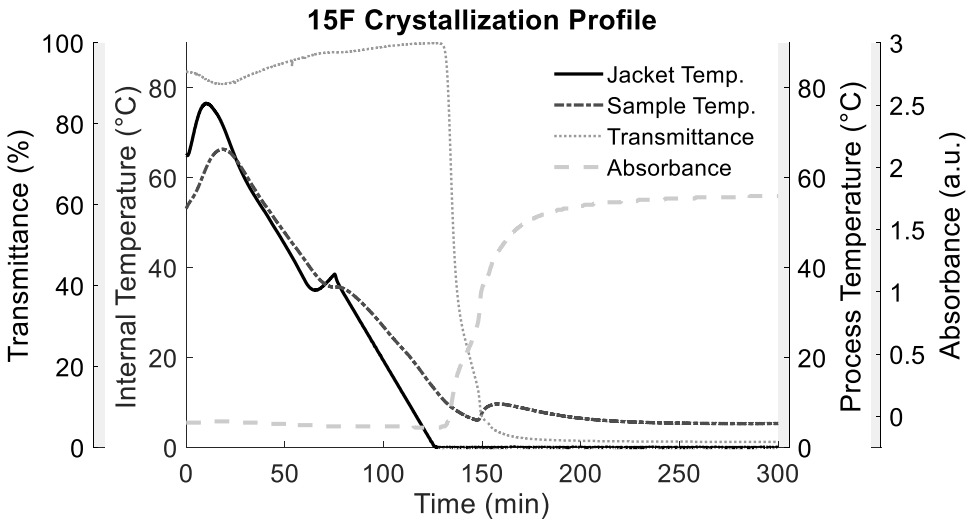

Figure 3. Crystallization of CB/HOSO oleogel with fast cooling rate at 15% CB by weight (15F). The Process Analytical Technologies (PAT) tools plot display the jacket temperature (-), sample temperature (-·-), light transmittance (···) and light absorbance (--) over time.

Soon after the crystallization onset, a temperature increase was observed for all oleogel samples, which was attributed to the latent heat of solidification for cocoa butter. Details of the crystallization process for each CB/HOSO mixture are summarised in Table 1. Due to the limited maximum heat transfer rate of the setup used, the temperature profile of the crystallizing mixtures did not follow the nominal cooling rates set for the experiments. The recalculated cooling rates are shown in Table 1.

Table 1. Cooling rates, crystallization temperatures, light absorbance and the measured increase in temperature recorded at the crystallization onset for oleogel samples prepared in this article.

Sample (oleogel)	Recalc. cooling rate (°C/min)	Crystallization temperature (°C)	Increase in temperature at nucleation (°C)	Absorbance at equilibrium (a.u.)
15F	-0.52 ± 0.08	11.0 ± 0.7	3.9 ± 0.7	1.99 ± 0.15
15M	-0.20 ± 0.02	10.5 ± 1.5	3.3 ± 0.3	2.13 ± 0.17
15S	-0.08 ± 0.01	9.5 ± 0.6	2.7 ± 0.2	2.21 ± 0.30
22F	-0.51 ± 0.04	13.2 ± 0.8	3.3 ± 1.7	2.41 ± 0.11
22M	-0.19 ± 0.02	12.5 ± 0.1	4.5 ± 0.8	2.56 ± 0.06
22S	-0.08 ± 0.01	13.2 ± 0.8	3.6 ± 1.1	2.62 ± 0.09
30F	-0.46 ± 0.08	15.7 ± 0.4	6.2 ± 0.8	2.73 ± 0.14
30M	-0.18 ± 0.02	14.8 ± 0.8	4.3 ± 0.9	2.76 ± 0.05
30S	-0.08 ± 0.01	15.0 ± 0.6	4.2 ± 0.6	2.87 ± 0.05

The recalculated cooling rate was *ca.* –0.50 °C/min for a nominal value of –0.75 °C/min, *ca.* –0.20 °C/min for a set rate of –0.25 °C/min and –0.08°C/min instead of –0.10 °C/min. The composition of the mixture, which affects the specific heat capacity and viscosity of the crystallizing oleogel, also affected the actual cooling rate. For fast cooling experiments the recalculate cooling rates were –0.46 °C/min for sample 30F, –0.51 °C/min for sample 22F and –0.52 °C/min for sample 15F. As shown in Table 1 the nucleation temperature of oleogels was mainly affected by the concentration of cocoa butter, whereas the cooling rate did not significantly affect it. The effect of using a larger processing volume and applying shear on the kinetic of crystal nucleation is evident upon comparison with the experiments described in the previous section.

388 Within small capillaries, the nucleation of oleogels was observed between 10 °C and 7 °C for all
389 the CB concentration investigated, whereas in the lab-scale vessel the crystallization temperature
390 was between approximately 10 and 15 °C. As shown in Figure 3, the emergence of CB crystals
391 coincided with an increase in temperature, indicating that primary nucleation of CB is an
392 exothermic process. The measured increase in temperature was between 3 and 6 °C and directly
393 proportional to the amount of CB in the CB/HOSO mixture. With regards to the measured
394 absorbance at equilibrium, its value was found to be roughly proportional to the amount of cocoa
395 butter in the crystallizing oleogel. In fact, the absorbance value from turbidity measurements is
396 directly proportional to the number of particles suspended in the continuous phase. However, shape
397 and size distributions can also affect this parameter and this might explain the differences in final
398 absorbance values for experiments carried out at different cooling rates[40]. At the end of the
399 crystallization process, all oleogels reached a final, constant temperature of *ca.* 7 °C.
400 Polarized light microscopy images of the oleogel sample obtained in this set of experiments are
401 shown in Figure 4.

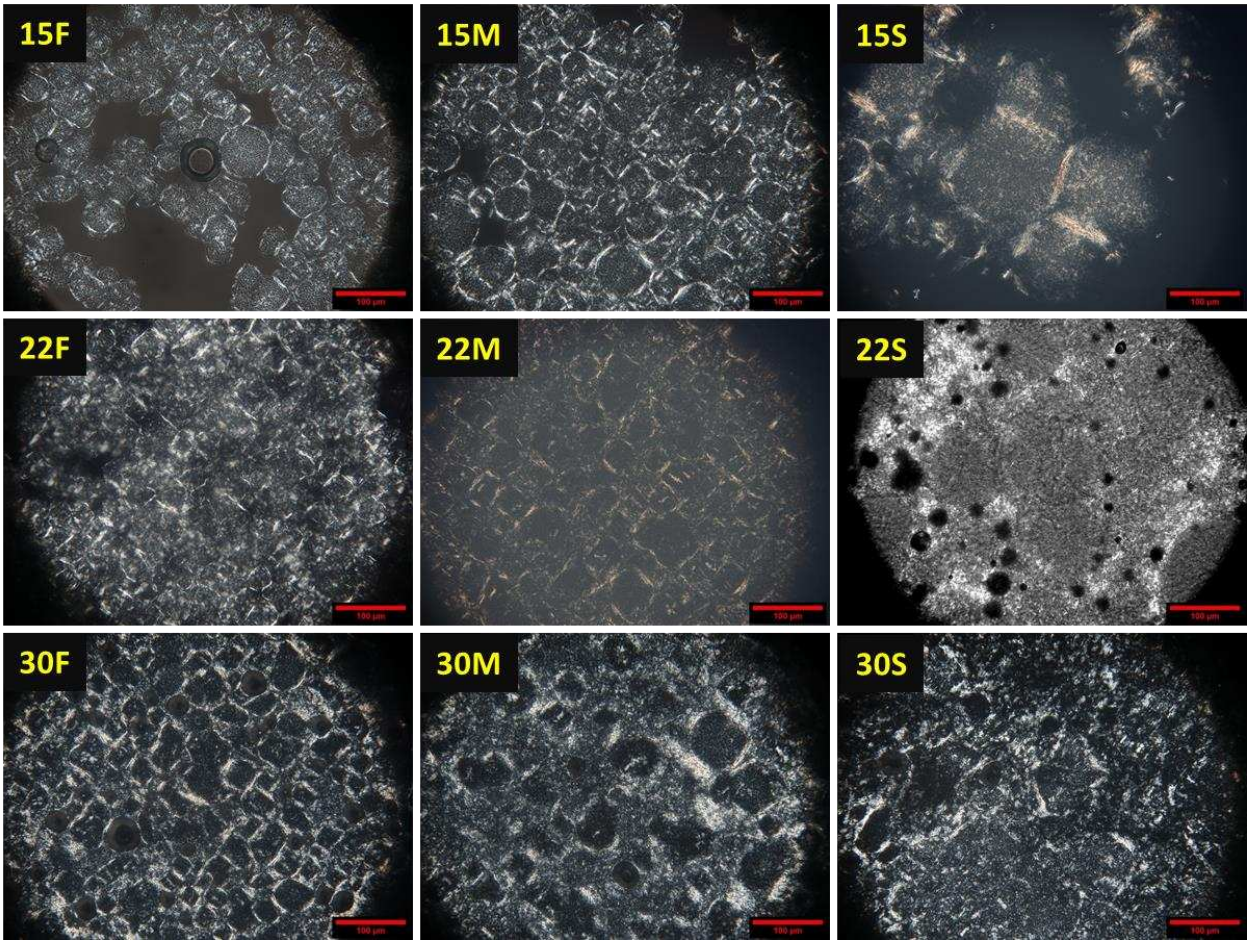

Figure 4. Polarized light images of oleogel samples investigated in this paper. Scale bar represents 100 μm.

Cocoa butter crystallized as spherical aggregates, which is the typical morphology for TAGs obtained using moderate to slow cooling rates, either in quiescent conditions[42,43] or under shear[44,45]. These crystalline aggregates are formed through the nucleation of nanometre-sized crystal nanoplatelets, followed by radial growth from the centre of the aggregate[46-47]. In particular, such crystal morphology was previously observed both in quiescent conditions in blends of cocoa butter and vegetable oils (soybean and canola oil)[38-39], and in dynamic crystallization conditions for a fully hydrogenated soybean oil (FHSO) in soybean oil (SO) mixture[44] and in fully

hydrogenated canola oil (FHCO) in canola oil (CO) system[45]. In both systems it was observed that the size of the spherical aggregates decreased with increasing shear rate.

Figure 4 shows oleogel samples containing a network of spherical aggregates entrapping the sunflower oil, which appeared dark under polarized light. Table 2 shows the average diameter size for the individual spherical aggregate in the oleogel samples, as measured manually from the microscopic images.

Table 2. Mean diameter of the spherical aggregates measured by image analysis of polarized light images of oleogels.

Sample (oleogel)	CB w/w %	Recalc. cooling rate (°C/min)	Spherical aggregates average diameter (µm)
15F	15	-0.52 ± 0.08	40.34 ± 7.89
22F	22	-0.51 ± 0.04	46.41 ± 12.08
30F	30	-0.46 ± 0.08	39.43 ± 9.98
15M	15	-0.20 ± 0.02	56.24 ± 13.78
22M	22	-0.19 ± 0.02	52.27 ± 11.05
30M	30	-0.18 ± 0.02	63.29 ± 12.41
15S	15	-0.08 ± 0.01	118.44 ± 32.42
22S	22	-0.08 ± 0.01	151.77 ± 51.58
30S	30	-0.08 ± 0.01	n/a

As a reference, an image focused on a single spherical aggregate is available in Supporting Information 2, showing how these crystal aggregates were measured with image analysis (Figure

S1). Fast-cooled samples (15F, 22F and 30F) presented spherical aggregates of around 40 µm in diameter, while medium (15M, 22M and 30M) and slow (15S and 22S) cooled samples showed larger aggregates of 50-60 µm and 100-150 µm respectively. The measurement of the size of the spherical aggregates in sample 30S (Figure 4, bottom right) was not possible, as this sample displayed a continuous network of crystalline CB where the edges of each aggregate could not be distinguished unambiguously. Slow cooling rates caused nucleation to happened at lower levels of undercooling compared to fast cooling rates, which promoted crystal growth over nucleation[48]. Therefore, the average diameter of crystalline spherical aggregates in the oleogels increased as the cooling rate decreases. The concentration of CB did not appear to affect significantly the average spherical aggregate diameter; however, it can be seen from Figure 4 that the number of spherical aggregates dispersed in sunflower oil increased with increasing CB concentration.

Cocoa butter polymorphism in oleogels was determined with X-Ray diffraction; samples were collected prior to aeration and their diffraction patterns are shown in Figure 5.

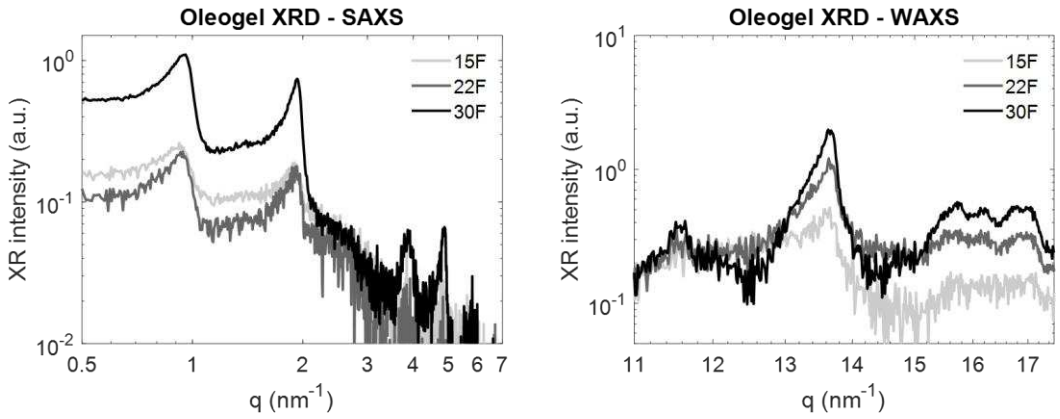

Figure 5. Solvent-subtracted X-Ray diffraction patterns of oleogel samples 15F, 22F and 30F prior to aeration.

All oleogels displayed two intense peaks in the small angle region at q values of around 0.96 nm^{-1} and 1.9 nm^{-1}, and in the wide-angle region a peak at around 13.7 nm^{-1} and a series of low-intensity peaks between 15.7 and 17.1 nm^{-1}. These peaks correspond to the β(V) cocoa butter polymorph[41]. The more metastable α and β'(IV) forms detected in the capillary experiments showed in the previous section were not detected. This can be explained by evaluating several factors that affected the lab scale crystallization of the oleogel samples. Application of shear during fat crystallization promotes faster polymorphic transformation, as shear-induced viscous heat generation can melt the less stable polymorphs, while leaving behind and provide the thermal energy to overcome the activation barrier for nucleation of the more stable structures[49]. Specifically, shear was reported to accelerate the transition of cocoa butter crystals from β'(IV) to β(V)[50]. In the experiments shown here, X-Ray diffraction was performed immediately at the end of each crystallization process; therefore, it is possible that lower-stability CB polymorphs that might have nucleated first transformed into the observed β(V) structure under the effect of shear. Furthermore, shear favours the secondary nucleation of stable polymorphs by enhancing crystal-crystal, crystal-impeller and crystal-vessel wall collisions[33]. In quiescent conditions, such as the capillary experiments described in the previous section, the reduced volume and the absence of shear-induced flow favoured primary over secondary nucleation instead, with unstable polymorphs being more persistent compared to large-scale crystallizers[51]. Lastly, the increase in temperature observed for oleogels soon after the crystallization onset (Figure 3) could have triggered a melt-mediated transformation of the nucleated metastable α or β'(IV) crystals to the detected β(V) polymorph.

The presence of a single crystal structure of CB in the oleogel samples was also supported by DSC measurements. A broad melting peak endotherm was observed for all oleogels between 20

and 30°C, whose position and intensity increased with CB concentration in the sample. The onset and maximum temperatures of the melting peaks of all analysed oleogels are shown in Table 3. A broad melting endotherm is characteristic of multi-component mixtures of fats, where TAGs with different fatty acid moieties form eutectic phases upon solidification[25]. Pérez-Martínez et al. (2012) reported similar DSC thermograms for a 30% w/w cocoa butter in soybean oil oleogel, crystallized under shear in a surface-scraper heat exchanger[52].

Table 3. Temperature of melting onset and peak melting temperature of oleogel samples.

Sample (oleogel)	T_{onset} oleogel (°C)	T_m oleogel (°C)
15F	21.34 ± 0.18	25.55 ± 0.92
15M	21.44 ± 0.27	24.07 ± 0.3
15S	21.54 ± 0.35	25.06 ± 0.82
22F	21.79 ± 0.42	26.17 ± 0.07
22M	20.91 ± 0.25	25.41 ± 0.34
22S	21.64 ± 0.02	26.25 ± 0.53
30F	21.90 ± 0.11	28.83 ± 1.82
30M	22.32 ± 0.06	28.08 ± 0.86
30S	21.37 ± 0.08	28.03 ± 1.02

The viscoelastic properties of the oleogel samples were investigated with oscillatory rheology at 20°C (Figure 6). Rheology profiles of medium and slow-cooled samples are available in Supporting Information 3.

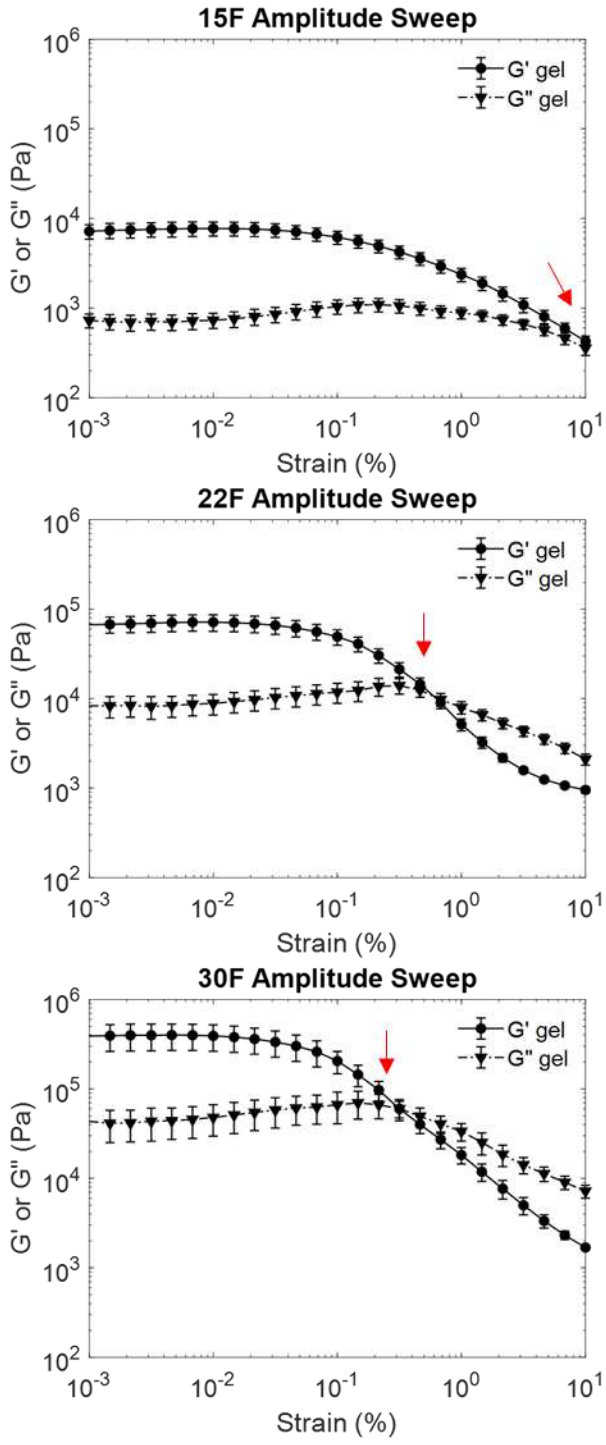

Figure 6. Oscillatory rheology of fast-cooled oleogels crystallized in the lab-scale vessel. Elastic modulus (G') and viscous modulus (G") are plotted as a function of strain (%). The flow point (τ_f) is highlighted with a red arrow.

The CB/HOSO oleogels prepared in this work exhibited predominantly elastic behaviour in the range 0.001 – 1% strain, after which they started to flow like liquid materials. Table 4 contains the oleogels' elastic modulus in the linear viscoelastic regime (G'_{LVER}) and the flow point (τ_f), which corresponds to the crossing point of the G' and G" curves.

Table 4. Elastic modulus in the linear viscoelastic regime (G'_{LVER}) and flow point (τ_f) of oleogel samples.

Sample	Oleogel G'_{LVER} (kPa)	Oleogel τ_f (kPa)
15F	7.52 ± 0.20	0.78 ± 0.39
15M	7.69 ± 0.07	0.46 ± 0.14
15S	9.16 ± 0.18	0.50 ± 0.12
22F	69.67 ± 1.82	16.55 ± 5.45
22M	71.21 ± 1.12	8.28 ± 0.85
22S	56.24 ± 0.59	11.89 ± 5.82
30F	396.14 ± 3.79	44.53 ± 15.50
30M	497.99 ± 6.66	49.72 ± 3.55
30S	472.31 ± 5.76	55.35 ± 3.42

The value of G'_{LVER} increased with increasing of CB concentration from 10^4 Pa to 10^6 Pa (Table 4), which is in agreement with the increasing amount of crystalline cocoa butter in the oleogels, as highlighted by DSC measurements. The flow point of the oleogels (τ_f) followed the same trend, increasing logarithmically from *ca.* 0.5 kPa to 50 kPa between 15% and 30% CB w/w. The size of

CB crystal aggregates, on the other hand, did not affect significantly the rheology of oleogels, which exhibited similar viscoelastic profiles at fixed concentration of CB (see Figure S2 in Supporting Information 3). As a comparison, Gunes et al. (2017) were able to aerate myristic acid – sunflower oil oleogels between with an elastic modulus between 10^3 Pa to 10^8 Pa[53].

Aeration of oleogels and characterization of oleofoams

The aeration profiles of oleogel samples and the temperature evolution during aeration are presented in Figure 7. Air incorporation was evident as all oleogels turned from a deep yellow to a white colour and mousse-like consistency. The oleogels prepared in this work exhibited high foamability, with an average overrun of 100% just after 5 minutes of aeration and up to 200% after 30 minutes or less. In comparison, the oleofoams prepared by Mishima et al. (2016), Gunes et al. (2017) and Heymans et al. (2018) required between 15 to 30 minutes aeration to surpass 100% overrun[29,31,53].

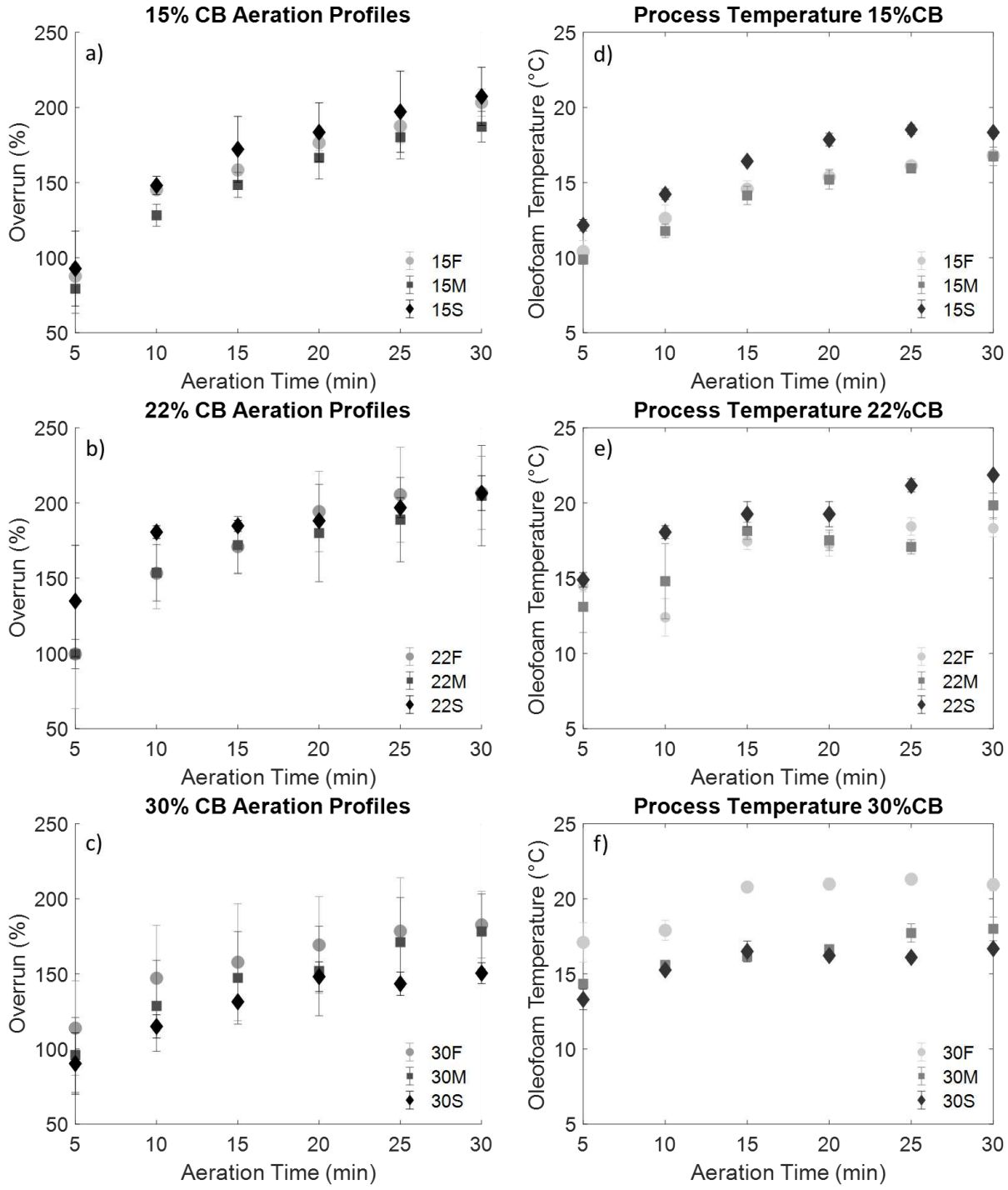

510

511 **Figure 7**. Foamability over time of oleofoams for 15% CB w/w, 22% CB w/w and 30% CB w/w

512 samples (a, b and c) and their temperature evolution during aeration (d, e and f).

513

For 15% CB w/w oleogels, air incorporation proceeded in a steady, stepwise fashion, without large variation in the mean overrun between different cooling rates. Oleogels containing 22% CB w/w displayed slightly higher overrun values over the first 10-15 minutes, potentially due to the larger amount of crystals available for bubble stabilization. In particular, sample 22S reached about 175% overrun after just 10 minutes of aeration, and maintained, on average, a similar overrun afterwards. This suggests that this sample reached air incorporation equilibrium after 10 min of aeration. While the relatively large error bars point to a high degree of variability, the mean overrun value increased just slightly after this time. The aeration of 30% CB w/w oleogels was less efficient; in fact, sections of unaerated oleogel were still visible at the end of the aeration process. Sample 30S, in particular, could only achieve a lower overrun (around 150%) compared to all the other samples. This observation suggests that, for CB/HOSO oleogels, 30% CB might be close to the upper limit of processability for aeration with the setup used in this work, due to their higher elastic modulus compared to the other samples. Previous experiments on the aeration of oleofoams prepared from 10% CB w/w oleogels, on the other hand, displayed good foamability, but also significant oil drainage shortly after the whipping. This confirms that the lower limit of CB concentration in HOSO was 15% w/w.

The temperature of every sample during aeration was also monitored with an external thermometer, as shown Figure 7d – 7f. The shear-induced viscous heat generation was partly counterbalanced by the cooling liquid flowing in the vessel jacket, which was kept at a constant temperature of 0°C. Nevertheless, all oleogel samples displayed an increase in temperature from *ca.* 7°C (the final crystallization temperature shown in Figure 3) to 10 – 15°C after 5 minutes of aeration. Throughout the rest of the whipping process, the oleofoams were heated gradually by a further 5 – 10 °C after 30 minutes of whipping, reaching a maximum temperature of 20°C.

Such increase in temperature is sufficient to dissolve the smaller CB crystals, and affect the morphology and size distribution of spherical aggregates, as well as the strength of the crystalline network for samples at 30% CB w/w. This can help explaining why sample foamability was mainly affected by the amount of cocoa butter crystals in the oleogels, rather than the cooling rate at which oleogel were formed. As shown in the previous sections, slower cooling rates promote the growth or fewer and larger crystals in the oleogels in comparison to faster cooling. Figure 8 contains polarized micrographs of oleofoams at the end of the aeration process, which shows that the concentration, size and shape of the cocoa butter crystals is very similar for samples containing the same amount of CB. The cocoa butter crystals appeared as bright objects in between air bubbles. It can be noticed that the size and shape distributions of both air bubbles and CB spherical aggregates in the oleofoams seem to be affected exclusively by the content of CB, with the only exception of sample 30S that, as mentioned earlier, was very difficult to aerate. It is likely that the increase in temperature during aeration, in combination with the mechanical breaking action of the mixer, can disrupt the crystalline network and reduce the size of large CB aggregates within the oleogels, resulting in very similar size and shape distributions of crystal aggregates in all whipped samples containing the same amount of CB. In other words, the aeration process seems to eliminate the effect of using different cooling rates in the formation of oleogels.

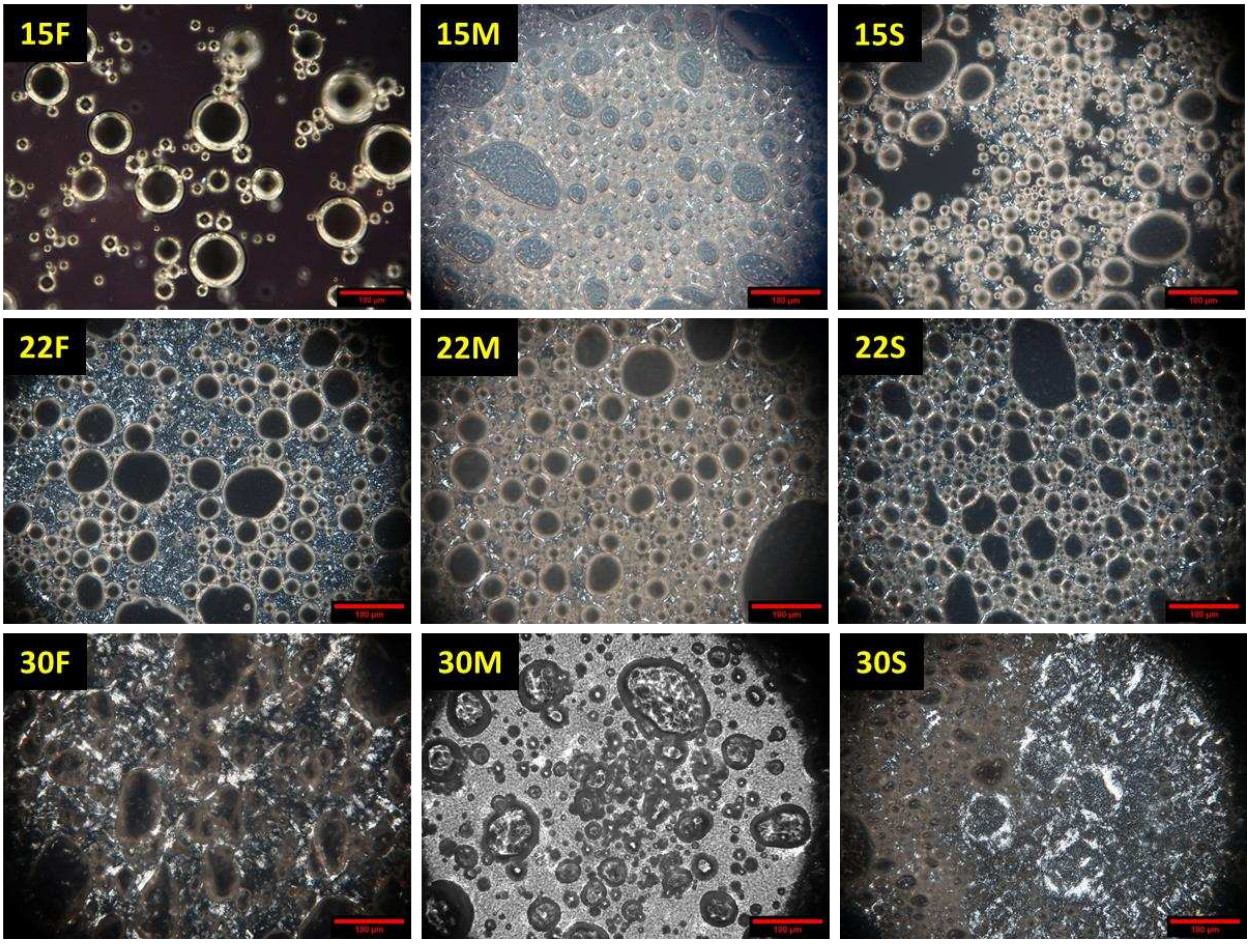

Figure 8. Polarized light images of oleofoam samples at the end of the aeration step. Scale bar represents 100µm.

Air bubbles had an estimated diameter between 5 and 100 µm, with several bubbles being non-spherical, which is common for these type of materials[28–31,35,53]. Oleofoam samples with 15% CB w/w contained more loosely dispersed bubbles, with more rounded shape and large domains of the foam did not present any crystal or bubble but were dominated by HOSO. In contrast, oleofoams prepared with 22% CB w/w displayed a more compact packing of non-spherical air bubbles, with a network of crystals in between the air bubbles. Samples with 30% CB w/w displayed a coarser microstructure, with fewer, larger, and more deformed air bubbles, as well as large domains of

564 crystal aggregates. The latter observation was in agreement with the lower overrun and
565 macroscopically visible traces of un-whipped material.

566 CryoSEM was used to resolve the structure of CB crystals in the oleofoam samples.
567 Furthermore, the ability to freeze-fracture the sample allowed to visualize the foam microstructure
568 closer to the native state compared to PLM, where oleofoams are subject to deformation during
569 sample preparation. Figure 9 shows the microstructure of a 30F oleofoam, which presented several
570 bubbles tightly packed and separated by thin layers of frozen oleogel (shown in Figure 9a).

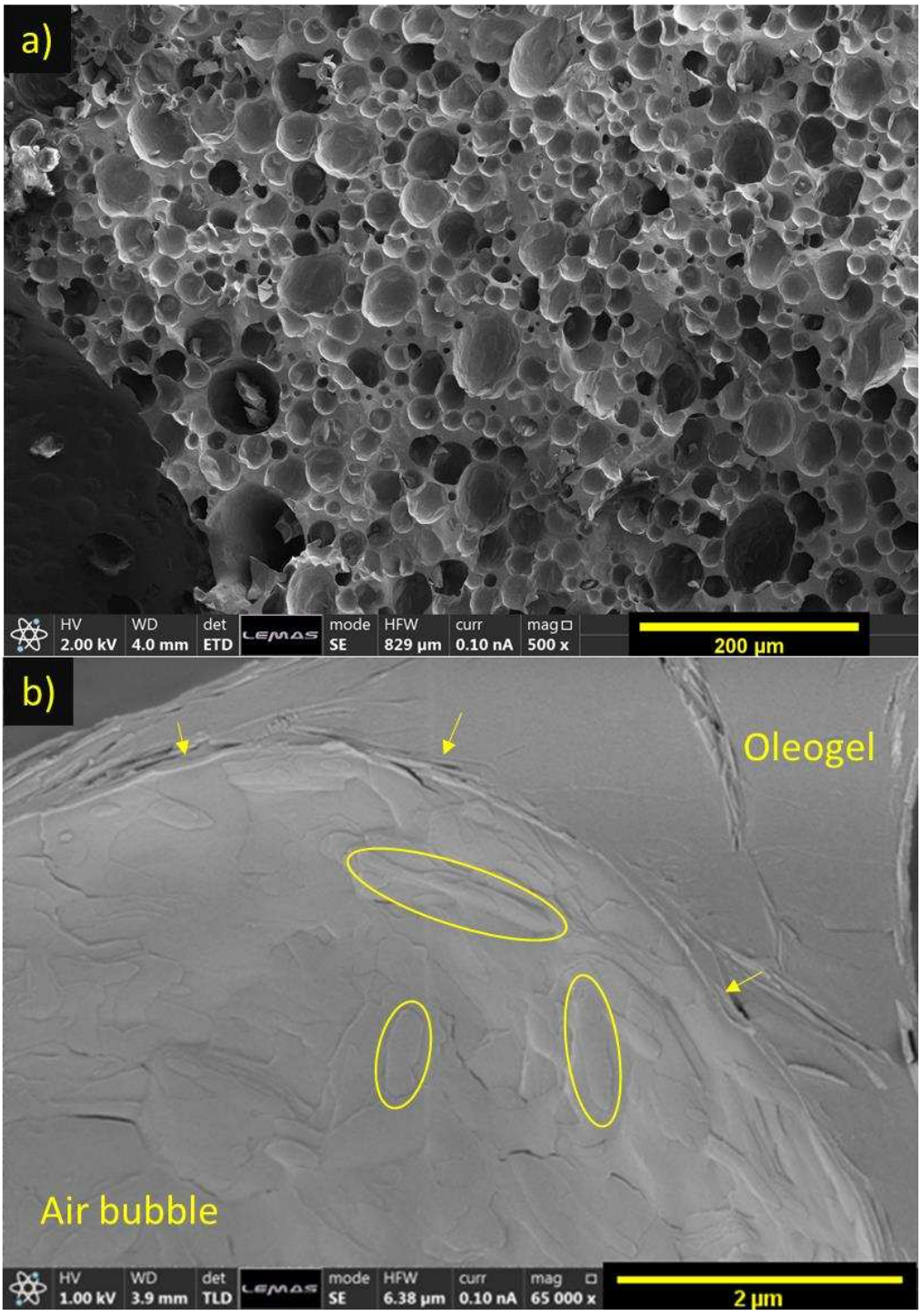

571

572 **Figure 9**. CryoSEM images of an oleofoam sample (30F). Low magnification (top, a), high
573 magnification with detail of the inside of an air bubble (bottom, b). The scale bars represent 200
574 µm and 2 µm, respectively.

575 The bubble diameter was found to be between 5 and 150 μm, similar to the range measured by
576 PLM. Figure 9b shows the inside of an air bubble at higher magnification. Cocoa butter
577 nanoplatelets (CNP) that form the spherical aggregates observed with PLM were detected both at
578 the interface and in the continuous phase of the oleofoams. The CNPs had a variable length
579 between 400 nm and 1 μm, as highlighted in Figure 9b by the yellow circles, and an approximate
580 thickness of *ca.* 50 nm. Further CryoSEM images are provided in Supporting Information 5
581 (Figures S5 – S8).
582 For all oleofoam samples, XRD and DSC measurements confirmed that these CB crystals were
583 the same polymorph, β(V), as the one found in the parent oleogels (Figure S4 in Supporting
584 Information 4). It can be noticed that CNPs are all exposing their larger facet at the air/oil interface
585 as shown with the yellow arrows in Figure 9b. The presence of bundles of CNPs within the oleogel
586 surrounding bubbles is also evident in Figure S5-S6 of Supporting Information 5.
587 This crystalline arrangement around air bubbles supports the hypothesis of a Pickering
588 stabilization mechanism, where CB crystals are adsorbed at the air/oil interfaces providing
589 stabilization from coalescence and coarsening[20,24]. The presence of a birefringent layer
590 surrounding bubbles confirms the presence of absorbed crystals at the air/oil interface, as shown
591 in the PLM images of Figure S9 in Supporting Information 6. Therefore, the crystal-stabilized air
592 bubbles form a network through the presence of additional CNPs in the continuous phase, which
593 also entrap the liquid oil. This hypothesis is also in agreement with the findings of Mishima et al.
594 (2016), Binks et al. (2016), Binks & Marinopoulos (2017) and Heymans et al. (2018) for similar
595 oleofoams[28,29,31,35]. The stabilization mechanism of the oleofoam investigated in this work is
596 summarized in Figure 10.

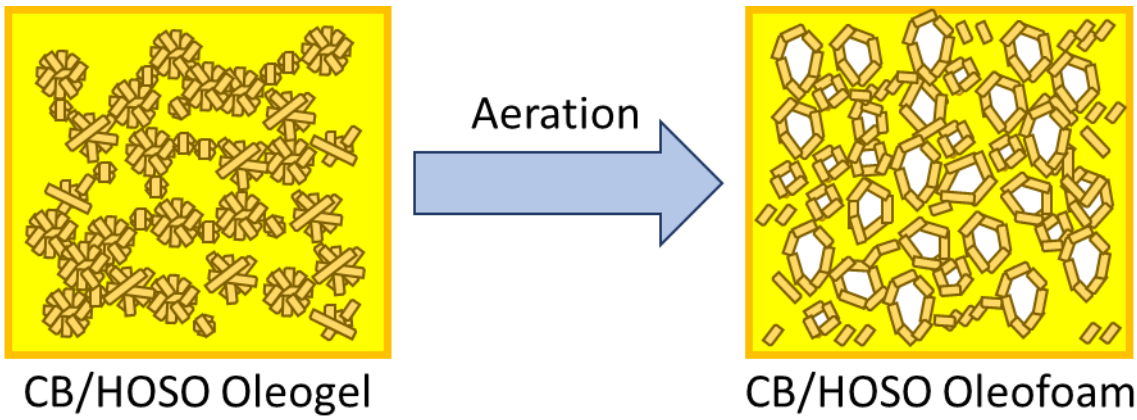

Figure 10. Diagram summarizing the effect of aeration on the cocoa butter oleogels prepared in this work. The spherical CB crystals aggregates in the oleogels are disrupted during the aeration producing a novel structure comprising of crystal-stabilized air bubbles interconnected in a fat-crystal network that entraps liquid oil as well.

The viscoelastic properties of oleofoams were investigated with oscillatory rheology. The elastic (G') and viscous (G") moduli of selected oleofoams are shown in Figure 11, compared with their relative oleogel precursors.

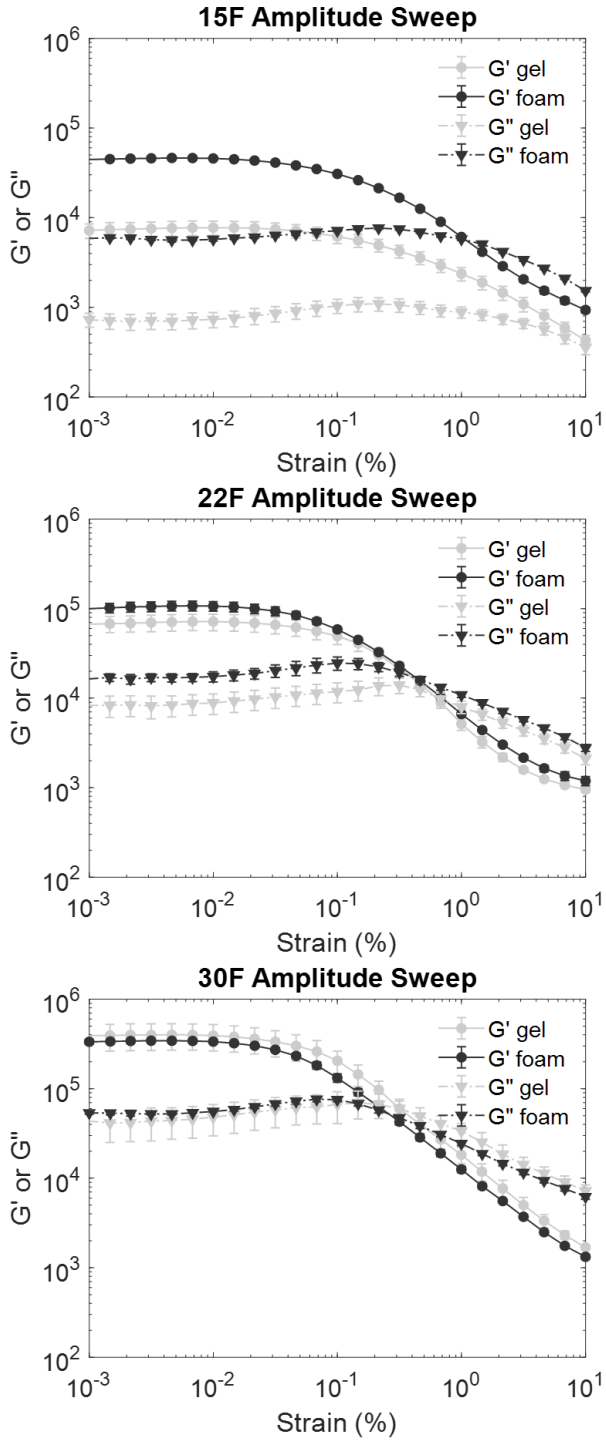

606

607 **Figure 11**. Oscillatory rheology experiments of fast-cooled oleofoam samples (grey) compared to

608 the results for their analogue oleogel samples (black).

609

610 Similarly to oleogel samples, oleofoams behaved as solid-like materials in a strain range between
611 0.001% and 1%, after which they started flowing like a liquid. Their G'_{LVER} increased with the CB
612 concentration, as seen in the oleogel analogues. The aeration process resulted in increased G' and
613 G" for oleofoams containing 15% and 22% CB w/w, while for samples containing 30% CB w/w
614 both elastic and viscous moduli decreased slightly compared to the originating oleogels. Therefore,
615 at low CB concentrations, the structural changes in oleogels caused by aeration led to a stronger
616 (*i.e.* with higher elastic modulus) material compared to the starting oleogels, as reported also by
617 Gunes et al. (2017) for oleofoams prepared with 5% w/w monoglyceride crystals in oil[53]. This
618 effect became less pronounced in samples with 30% CB w/w, whose oleofoams presented a
619 viscoelastic profile very similar to their oleogel precursors. A possible explanation could be that,
620 for oleofoams prepared from 30% w/w cocoa butter oleogels, the crystal rearrangement around the
621 air bubbles did not contribute significantly to the rheology of the material, both due to the lesser
622 extent of air incorporated and to the presence of a stronger fat crystal network, as highlighted by
623 the higher elastic modulus compared to 15% w/w and 22% w/w samples. It is worth noticing that
624 the variation of G' and G" was affected mostly by the different CB concentrations in the originating
625 oleogels, as the amount of incorporated air was relatively similar between the oleofoam samples
626 (see Supporting Information 7, Figure S10). In fact, the air volume fraction was around 0.66 for
627 samples containing 15% and 22% CB w/w, 0.64 for samples 30M and 30F and 0.60 for sample
628 30S. More details are provided in Table 5, which contains the flow point of oleofoams, their
629 overrun, and the ratio between the G'_{LVER} of oleofoams and their respective oleogels.
630 A comparison of the values shown in Tables 4 and Table 5 shows that whipping of CB/HOSO
631 oleogels with 15% CB w/w increased both elastic and viscous moduli by a factor of 4 to 6 G'_{LVER}
632 and generated an increase in volume of 200% compared with the oleogel precursors. Oleofoam

633 samples with 22% CB w/w showed a smaller increase of G'_{LVER} (1.5 to 2 times), and an average
634 volume increase of 200%. Finally, oleofoams with 30% CB w/w exhibited a modest decrease of
635 G'_{LVER} after aeration (0.85 to 0.92 times), still incorporating high amounts of air bubbles, with
636 overrun values between 150% and 180%. As a reference, Binks & Marinopoulos (2017) reported
637 that aeration of pure cocoa butter at 35°C – with a solid fat content between 15 and 30% – resulted
638 in an oleofoam with 100% overrun[35].
639
640 **Table 5**. Linear Viscoelastic Regime (LVER) elastic modulus, viscous modulus, and flow points
641 for oleofoams investigated in this paper.

Sample	Oleofoam G'_{LVER} (kPa)	Oleofoam τ_f (kPa)	Overrun (%)	Foam G'_{LVER}/Gel G'_{LVER}
15F	45.63 ± 0.64	4.77 ± 1.00	203 ± 9	6.06
15M	31.37 ± 0.32	4.57 ± 0.06	187 ± 10	4.07
15S	45.65 ± 0.60	6.91 ± 0.35	207 ± 19	4.98
22F	104.79 ± 2.84	21.93 ± 6.28	206 ± 24	1.50
22M	111.26 ± 2.40	11.07 ± 9.59	204 ± 33	1.56
22S	111.22 ± 1.47	19.53 ± 3.56	207 ± 16	1.97
30F	339.83 ± 3.71	40.67 ± 11.68	182 ± 22	0.85
30M	438.21 ± 7.52	56.38 ± 6.80	178 ± 25	0.88
30S	453.21 ± 5.75	60. 21 ± 13.03	150 ± 7	0.92

642
643 **Oleofoam stability studies**
644 Oleofoams are subject to the same destabilisation mechanisms found in aqueous foams, such as
645 liquid drainage, bubble coalescence and coarsening. Specifically, oil drainage from the continuous

phase causes film thinning between the bubbles, with increased probability of coalescence[20,54]. Nevertheless, the oleofoam samples studied in this work did not display measurable amounts of oil drainage (< 1 mL over 50 mL of sample) over 3 months (as shown in Figure S11 of Supporting Information 8). This is in agreement with the behaviour of other stable oil foam systems reported in literature[29,35,53]. A comparison between fresh and aged oleofoam samples was carried out using CryoSEM. This analysis showed that air bubbles retained a non-spherical shape during aging, as well as the presence of CNPs at the air/oil bubble boundary. The aged sample displayed fewer bubbles in the bulk, as shown in Figure S12 of Supporting Information 9.

CONCLUSIONS

In the present work, the complex relationship between processing conditions and the physiochemical properties of oleogels and oleofoams was explored with a multiple characterization technique approach. Specifically, the effect of CB crystal size and shape distributions on the final oleofoam properties was determined. These results are relevant to Pickering-stabilized oleofoam; more specifically, for industries who seek to use oleofoams in their products and to implement them in their manufacturing processes. For them, being able to generate oleogels with tailored-made crystal properties is the key to produce highly aerated, stable oleofoams with desirable viscoelastic properties.

The oleofoams prepared in this work were found to be Pickering-stabilized by CB nanoplatelets in the β(V) polymorph, and were able to incorporate an air volume fraction of $\varphi = 0.60$ to $\varphi = 0.66$. CryoSEM allowed to visualize the CB crystals at the air/oil interface in the oleofoams. CB crystals appeared platelet-shaped with an estimated thickness of 50 nm and up to 500 nm in length, forming a layered shell of oriented crystals around the air bubbles. This resulted in oleofoams having up to

669 1/3 of the calorific density compared to their oleogel precursors, which is beneficial for
670 formulating products with lower calories. Moreover, the oleofoams were stable to oil drainage for
671 up to 3 months at 20°C. The concentration of CB was the factor that affected more strongly the
672 properties of both oleogels and oleofoams. In particular, by tuning the amount of CB in the
673 oleogels, oleofoams with either higher or similar viscoelasticity to the oleogel could be produced.
674 Oleogels containing spherical crystal aggregates of different size produced oleofoams with similar
675 properties, as the aeration processes eliminated all differences in crystal size and shape
676 distributions generated by applying different cooling rates during the oleogel formation. In this
677 work the effect of shear and increased volume on the crystallization of CB/HOSO blends was also
678 elucidated by comparing oleogel crystallization in quiescent capillaries and in a stirred lab-scale
679 crystallization vessel. The use of online, *in* situ light turbidimetry allowed to monitor the process
680 dynamic of oleogels crystallization and to identify when the system reached equilibrium at the end
681 of the cooling profile.
682 The CB-based oleofoams obtained in this work are relevant, novel materials that can promote
683 the reformulation of healthier, more affordable and sustainable food products, such as fillings and
684 chocolate spreads. Furthermore, they constitute also attractive scaffolds for cosmetic (*e.g.*
685 skincare) products, as well as carriers for active pharmaceutical ingredients.
686
687 ASSOCIATED CONTENT

688 **Supporting Information**. Additional images, X-ray diffraction patterns of oleogels and
689 oleofoams are provided in the Supporting Information together with details of the data processing
690 of X-ray patterns and additional data collected during crystallization experiments (e.g., evolution
691 of air incorporation, microscopy images).

692

693 AUTHOR INFORMATION

694 Corresponding Author

695 **Corresponding author:* *e.simone@leeds.ac.uk*, +44(0)113 343 1424

696

697 **Funding Sources**

698 The authors would like to acknowledge the Engineering and Physical Sciences Research Council
699 funded Centre for Doctoral Training in Soft Matter and Functional Interfaces, grant ref. no.
700 EP/L015536/1 as well as Nestlé PTC Confectionery (York, UK) for the financial and writing
701 support. Dr Simone also acknowledges Royal Society (grant ref. no. INF\R2\192018) for
702 additional funding. Additional financial support was provided by Diamond Light Source (Didcot,
703 UK) through proposals SM24530-1, SM22659-1 and SM20481-1 at beamline I22.

704

705 **Notes**

706 The authors declare that they have no known competing financial interests or personal
707 relationships that could have appeared to influence the work reported in this paper.

708

709 ACKNOWLEDGMENT

710 Dr Arwen Tyler, Prof Megan Povey and Prof Michael Rappolt are acknowledged for useful
711 discussion on X-Ray data and cocoa butter polymorphism. Dr. Daniel Baker is acknowledged for
712 his support on DSC measurements and data analysis. Dr. Teresa Roncal-Herrero and Mr. Stuart

Micklethwaite are also acknowledged for their support in CryoSEM microscopy and data analysis. We also thank Prof. Nick Terrill and Dr Andy Smith from Diamond Light Source for their support and assistance in running synchrotron experiments.

ABBREVIATIONS

CB Cocoa Butter, HOSO High Oleic Sunflower Oil, PAT Processing Analytical Technologies

REFERENCES

(1) Afshin, A.; Forouzanfar, M. H.; Reitsma, M. B.; Sur, P.; Estep, K.; Lee, A.; Marczak, L.; Mokdad, A. H.; Moradi-Lakeh, M.; Naghavi, M.; Salama, J. S.; Vos, T.; Abate, K. H.; Abbafati, C.; Ahmed, M. B.; Al-Aly, Z.; Alkerwi, A.; Al-Raddadi, R.; Amare, A. T.; Amberbir, A.; Amegah, A. K.; Amini, E.; Amrock, S. M.; Anjana, R. M.; Ärnlöv, J.; Asayesh, H.; Banerjee, A.; Barac, A.; Baye, E.; Bennett, D. A.; Beyene, A. S.; Biadgilign, S.; Biryukov, S.; Bjertness, E.; Boneya, D. J.; Campos-Nonato, I.; Carrero, J. J.; Cecilio, P.; Cercy, K.; Ciobanu, L. G.; Cornaby, L.; Damtew, S. A.; Dandona, L.; Dandona, R.; Dharmaratne, S. D.; Duncan, B. B.; Eshrati, B.; Esteghamati, A.; Feigin, V. L.; Fernandes, J. C.; Fürst, T.; Gebrehiwot, T. T.; Gold, A.; Gona, P. N.; Goto, A.; Habtewold, T. D.; Hadush, K. T.; Hafezi-Nejad, N.; Hay, S. I.; Horino, M.; Islami, F.; Kamal, R.; Kasaeian, A.; Katikireddi, S. V; Kengne, A. P.; Kesavachandran, C. N.; Khader, Y. S.; Khang, Y.-H.; Khubchandani, J.; Kim, D.; Kim, Y. J.; Kinfu, Y.; Kosen, S.; Ku, T.; Defo, B. K.; Kumar, G. A.; Larson, H. J.; Leinsalu, M.; Liang, X.; Lim, S. S.; Liu, P.; Lopez, A. D.; Lozano, R.; Majeed, A.; Malekzadeh, R.; Malta, D. C.; Mazidi, M.; McAlinden, C.; McGarvey, S. T.; Mengistu, D. T.; Mensah, G. A.; Mensink, G. B. M.; Mezgebe, H. B.; Mirrakhimov, E. M.; Mueller, U. O.; Noubiap, J. J.; Obermeyer, C. M.; Ogbo, F. A.; Owolabi, M. O.; Patton, G.

C.; Pourmalek, F.; Qorbani, M.; Rafay, A.; Rai, R. K.; Ranabhat, C. L.; Reinig, N.; Safiri, S.; Salomon, J. A.; Sanabria, J. R.; Santos, I. S.; Sartorius, B.; Sawhney, M.; Schmidhuber, J.; Schutte, A. E.; Schmidt, M. I.; Sepanlou, S. G.; Shamsizadeh, M.; Sheikhbahaei, S.; Shin, M.-J.; Shiri, R.; Shiue, I.; Roba, H. S.; Silva, D. A. S.; Silverberg, J. I.; Singh, J. A.; Stranges, S.; Swaminathan, S.; Tabarés-Seisdedos, R.; Tadese, F.; Tedla, B. A.; Tegegne, B. S.; Terkawi, A. S.; Thakur, J. S.; Tonelli, M.; Topor-Madry, R.; Tyrovolas, S.; Ukwaja, K. N.; Uthman, O. A.; Vaezghasemi, M.; Vasankari, T.; Vlassov, V. V; Vollset, S. E.; Weiderpass, E.; Werdecker, A.; Wesana, J.; Westerman, R.; Yano, Y.; Yonemoto, N.; Yonga, G.; Zaidi, Z.; Zenebe, Z. M.; Zipkin, B.; Murray, C. J. L. Health Effects of Overweight and Obesity in 195 Countries over 25 Years. *N. Engl. J. Med.* **2017**, *377* (1), 13–27. https://doi.org/10.1056/NEJMoa1614362.

(2) Ng, M.; Fleming, T.; Robinson, M.; Thomson, B.; Graetz, N.; Margono, C.; Mullany, E. C.; Biryukov, S.; Abbafati, C.; Abera, S. F.; Abraham, J. P.; Abu-Rmeileh, N. M. E.; Achoki, T.; Albuhairan, F. S.; Alemu, Z. A.; Alfonso, R.; Ali, M. K.; Ali, R.; Guzman, N. A.; Ammar, W.; Anwari, P.; Banerjee, A.; Barquera, S.; Basu, S.; Bennett, D. A.; Bhutta, Z.; Blore, J.; Cabral, N.; Nonato, I. C.; Chang, J. C.; Chowdhury, R.; Courville, K. J.; Criqui, M. H.; Cundiff, D. K.; Dabhadkar, K. C.; Dandona, L.; Davis, A.; Dayama, A.; Dharmaratne, S. D.; Ding, E. L.; Durrani, A. M.; Esteghamati, A.; Farzadfar, F.; Fay, D. F. J.; Feigin, V. L.; Flaxman, A.; Forouzanfar, M. H.; Goto, A.; Green, M. A.; Gupta, R.; Hafezi-Nejad, N.; Hankey, G. J.; Harewood, H. C.; Havmoeller, R.; Hay, S.; Hernandez, L.; Husseini, A.; Idrisov, B. T.; Ikeda, N.; Islami, F.; Jahangir, E.; Jassal, S. K.; Jee, S. H.; Jeffreys, M.; Jonas, J. B.; Kabagambe, E. K.; Khalifa, S. E. A. H.; Kengne, A. P.; Khader, Y. S.; Khang, Y. H.; Kim, D.; Kimokoti, R. W.; Kinge, J. M.; Kokubo, Y.; Kosen, S.; Kwan,

759 G.; Lai, T.; Leinsalu, M.; Li, Y.; Liang, X.; Liu, S.; Logroscino, G.; Lotufo, P. A.; Lu, Y.;
760 Ma, J.; Mainoo, N. K.; Mensah, G. A.; Merriman, T. R.; Mokdad, A. H.; Moschandreas, J.;
761 Naghavi, M.; Naheed, A.; Nand, D.; Narayan, K. M. V.; Nelson, E. L.; Neuhouser, M. L.;
762 Nisar, M. I.; Ohkubo, T.; Oti, S. O.; Pedroza, A.; Prabhakaran, D.; Roy, N.; Sampson, U.;
763 Seo, H.; Sepanlou, S. G.; Shibuya, K.; Shiri, R.; Shiue, I.; Singh, G. M.; Singh, J. A.;
764 Skirbekk, V.; Stapelberg, N. J. C.; Sturua, L.; Sykes, B. L.; Tobias, M.; Tran, B. X.;
765 Trasande, L.; Toyoshima, H.; Van De Vijver, S.; Vasankari, T. J.; Veerman, J. L.;
766 Velasquez-Melendez, G.; Vlassov, V. V.; Vollset, S. E.; Vos, T.; Wang, C.; Wang, X.;
767 Weiderpass, E.; Werdecker, A.; Wright, J. L.; Yang, Y. C.; Yatsuya, H.; Yoon, J.; Yoon, S.
768 J.; Zhao, Y.; Zhou, M.; Zhu, S.; Lopez, A. D.; Murray, C. J. L.; Gakidou, E. Global,
769 Regional, and National Prevalence of Overweight and Obesity in Children and Adults
770 during 1980-2013: A Systematic Analysis for the Global Burden of Disease Study 2013.
771 *Lancet* **2014**, *384* (9945), 766–781. https://doi.org/10.1016/S0140-6736(14)60460-8.

772 (3) Ruiz-Núñez, B.; Dijck-Brouwer, D. A. J.; Muskiet, F. A. J. The Relation of Saturated Fatty
773 Acids with Low-Grade Inflammation and Cardiovascular Disease. *J. Nutr. Biochem.* **2016**,
774 *36*, 1–20. https://doi.org/10.1016/j.jnutbio.2015.12.007.

775 (4) FAO. *Food and Agriculture Organizationof the United Nations, Fats and Fatty Acids in*
776 *Human Nutrition - Report of an Expert Consultation"*; 2008; Vol. 91.
777 https://doi.org/I1953E/1/11.10.

778 (5) EFSA. Scientific Opinion on Dietary Reference Values for Fats, Including Saturated Fatty
779 Acids, Polyunsaturated Fatty Acids, Monounsaturated Fatty Acids, Trans Fatty Acids, and
780 Cholesterol. *EFSA J.* **2010**, *8* (3), 1–107. https://doi.org/10.2903/j.efsa.2010.1461.

(6) McClements, D. J. Future Foods: A Manifesto for Research Priorities in Structural Design of Foods. *Food Funct.* **2020**, *11* (3), 1933–1945. https://doi.org/10.1039/c9fo02076d.

(7) Rios, R. V.; Pessanha, M. D. F.; Almeida, P. F. de; Viana, C. L.; Lannes, S. C. da S. Application of Fats in Some Food Products. *Food Sci. Technol.* **2014**, *34* (1), 3–15. https://doi.org/10.1590/s0101-20612014000100001.

(8) Ghotra, B. S.; Dyal, S. D.; Narine, S. S. Lipid Shortenings: A Review. **2002**, *35*, 1015–1048.

(9) Beg, M. S.; Ahmad, S.; Jan, K.; Bashir, K. Status, Supply Chain and Processing of Cocoa - A Review. *Trends Food Sci. Technol.* **2017**, *66*, 108–116. https://doi.org/10.1016/j.tifs.2017.06.007.

(10) Jahurul, M. H. A.; Zaidul, I. S. M.; Norulaini, N. A. N.; Sahena, F.; Jinap, S.; Azmir, J.; Sharif, K. M.; Mohd Omar, A. K. Cocoa Butter Fats and Possibilities of Substitution in Food Products Concerning Cocoa Varieties, Alternative Sources, Extraction Methods, Composition, and Characteristics. *J. Food Eng.* **2013**, *117* (4), 467–476. https://doi.org/10.1016/j.jfoodeng.2012.09.024.

(11) Patel, A. R.; Dewettinck, K. Edible Oil Structuring: An Overview and Recent Updates. *Food Funct.* **2016**, *7* (1), 20–29. https://doi.org/10.1039/c5fo01006c.

(12) Pehlivanoğlu, H.; Demirci, M.; Toker, O. S.; Konar, N.; Karasu, S.; Sagdic, O. Oleogels, a Promising Structured Oil for Decreasing Saturated Fatty Acid Concentrations: Production and Food-Based Applications. *Crit. Rev. Food Sci. Nutr.* **2018**, *58* (8), 1330–1341. https://doi.org/10.1080/10408398.2016.1256866.

(13) Demirkesen, I.; Mert, B. Recent Developments of Oleogel Utilizations in Bakery Products. *Crit. Rev. Food Sci. Nutr.* **2019**, *0* (0), 1–20. https://doi.org/10.1080/10408398.2019.1649243.

(14) Doan, C. D.; Patel, A. R.; Tavernier, I.; De Clercq, N.; Van Raemdonck, K.; Van de Walle, D.; Delbaere, C.; Dewettinck, K. The Feasibility of Wax-Based Oleogel as a Potential Co-Structurant with Palm Oil in Low-Saturated Fat Confectionery Fillings. *Eur. J. Lipid Sci. Technol.* **2016**, *118* (12), 1903–1914. https://doi.org/10.1002/ejlt.201500172.

(15) Si, H.; Cheong, L. Z.; Huang, J.; Wang, X.; Zhang, H. Physical Properties of Soybean Oleogels and Oil Migration Evaluation in Model Praline System. *JAOCS, J. Am. Oil Chem. Soc.* **2016**, *93* (8), 1075–1084. https://doi.org/10.1007/s11746-016-2846-1.

(16) Patel, A. R.; Rajarethinem, P. S.; Gręd owska, A.; Turhan, O.; Lesaffer, A.; De Vos, W. H.; Van De Walle, D.; Dewettinck, K. Edible Applications of Shellac Oleogels: Spreads, Chocolate Paste and Cakes. *Food Funct.* **2014**, *5* (4), 645–652. https://doi.org/10.1039/c4fo00034j.

(17) Campbell, G. M.; Mougeot, E. Creation and Characterisation of Aerated Food Products. *Trends Food Sci. Technol.* **1999**, *10* (9), 283–296. https://doi.org/10.1016/S0924-2244(00)00008-X.

(18) Blom, W. A. M.; Koppenol, W. P.; Schuring, E. A. H.; Abrahamse, S. L.; Arnaudov, L. N.; Mela, D. J.; Stoyanov, S. D. Sustained Satiety Induced by Food Foams Is Independent of Energy Content, in Healthy Adults. *Appetite* **2016**, *97*, 64–71. https://doi.org/10.1016/j.appet.2015.11.023.

(19) Palzer, S. Technological Solutions for Reducing Impact and Content of Health Sensitive Nutrients in Food. *Trends Food Sci. Technol.* **2017**, *62*, 170–176. https://doi.org/10.1016/j.tifs.2016.11.022.

(20) Heymans, R.; Tavernier, I.; Dewettinck, K.; Van der Meeren, P. Crystal Stabilization of Edible Oil Foams. *Trends Food Sci. Technol.* **2017**, *69*, 13–24. https://doi.org/10.1016/j.tifs.2017.08.015.

(21) Z.D. Gunes, O. Schafer, H. Chisholm, H. Deyber, C. P. and B. P. B. Lipid Based Foam, 2016.

(22) H. Chisholm, Z.D. Gunes, C. Gehin-Delval, A. Nouzille, E. Garvey, M.J. Destribats, S.N. Chandrasekaran, J. Vieira, J. German and B.P. BinksH. Chisholm, Z.D. Gunes, C. Gehin-Delval, A. Nouzille, E. Garvey, M.J. Destribats, S.N. Chandrasekaran, J. Vieira, J. G. and B. P. B. Aerated Confectionery Material, 2016.

(23) Haedelt, J.; Beckett, S. T.; Niranjan, K.; Pyle, D. L. Food Engineering and Physical Properties Vacuum-Induced Bubble Formation in Liquid-Tempered Chocolate. **2005**, *70* (2), 159–164.

(24) Fameau, A. L.; Saint-Jalmes, A. Non-Aqueous Foams: Current Understanding on the Formation and Stability Mechanisms. *Adv. Colloid Interface Sci.* **2017**, *247*, 454–464. https://doi.org/10.1016/j.cis.2017.02.007.

(25) Himawan, C.; Starov, V. M.; Stapley, A. G. F. Thermodynamic and Kinetic Aspects of Fat Crystallization. **2006**, *122*, 3–33. https://doi.org/10.1016/j.cis.2006.06.016.

(26) Fameau, A. L.; Lam, S.; Arnould, A.; Gaillard, C.; Velev, O. D.; Saint-Jalmes, A. Smart

844 Nonaqueous Foams from Lipid-Based Oleogel. *Langmuir* **2015**, *31* (50), 13501–13510.
845 https://doi.org/10.1021/acs.langmuir.5b03660.

846 (27) Brun, M.; Delample, M.; Harte, E.; Lecomte, S.; Leal-Calderon, F. Stabilization of Air
847 Bubbles in Oil by Surfactant Crystals: A Route to Produce Air-in-Oil Foams and Air-in-
848 Oil-in-Water Emulsions. *Food Res. Int.* **2015**, *67*, 366–375.
849 https://doi.org/10.1016/j.foodres.2014.11.044.

850 (28) Binks, B. P.; Garvey, E. J.; Vieira, J. Whipped Oil Stabilised by Surfactant Crystals. *Chem.*
851 *Sci.* **2016**, *7* (4), 2621–2632. https://doi.org/10.1039/C6SC00046K.

852 (29) Mishima, S.; Suzuki, A.; Sato, K.; Ueno, S. Formation and Microstructures of Whipped
853 Oils Composed of Vegetable Oils and High-Melting Fat Crystals. *JAOCS, J. Am. Oil Chem.*
854 *Soc.* **2016**, *93* (11), 1453–1466. https://doi.org/10.1007/s11746-016-2888-4.

855 (30) Truong, T.; Prakash, S.; Bhandari, B. Effects of Crystallisation of Native Phytosterols and
856 Monoacylglycerols on Foaming Properties of Whipped Oleogels. *Food Chem.* **2019**, *285*
857 (January), 86–93. https://doi.org/10.1016/j.foodchem.2019.01.134.

858 (31) Heymans, R.; Tavernier, I.; Danthine, S.; Rimaux, T.; Van Meeren, P.; Dewettinck, K.
859 Food-Grade Monoglyceride Oil Foams: The Effect of Tempering on Foamability, Foam
860 Stability and Rheological Properties. *Food Funct.* **2018**, *9* (6), 3143–3154.
861 https://doi.org/10.1039/c8fo00536b.

862 (32) Toro-vazquez, J. F.; Charó-alonso, M. A.; Morales-rueda, J. A.; Pérez-martínez, J. D.
863 Molecular Interactions of Triacylglycerides in Blends of Cocoa Butter With; 2005; pp 393–
864 416.

(33) Agrawal, S. G.; Paterson, A. H. J. Secondary Nucleation: Mechanisms and Models. *Chem. Eng. Commun.* **2015**, *202* (5), 698–706. https://doi.org/10.1080/00986445.2014.969369.

(34) Liu, Y.; Binks, B. P. Foams of Vegetable Oils Containing Long-Chain Triglycerides. *J. Colloid Interface Sci.* **2021**, *583*, 522–534. https://doi.org/10.1016/j.jcis.2020.09.043.

(35) Binks, B. P.; Marinopoulos, I. Ultra-Stable Self-Foaming Oils. *Food Res. Int.* **2017**, *95*, 28–37. https://doi.org/10.1016/j.foodres.2017.02.020.

(36) Raß, M.; Schein, C.; Matthäus, B. Virgin Sunflower Oil. *Eur. J. Lipid Sci. Technol.* **2008**, *110* (7), 618–624. https://doi.org/10.1002/ejlt.200800049.

(37) Fernández-Moya, V.; Martínez-Force, E.; Garcés, R. Identification of Triacylglycerol Species from High-Saturated Sunflower (Helianthus Annuus) Mutants. *J. Agric. Food Chem.* **2000**, *48* (3), 764–769. https://doi.org/10.1021/jf9903861.

(38) Lipp, M.; Simoneau, C.; Ulberth, F.; Anklam, E.; Crews, C.; Brereton, P.; De Greyt, W.; Schwack, W.; Wiedmaier, C. Composition of Genuine Cocoa Butter and Cocoa Butter Equivalents. *J. Food Compos. Anal.* **2001**, *14* (4), 399–408. https://doi.org/10.1006/jfca.2000.0984.

(39) Filik, J.; Ashton, A. W.; Chang, P. C. Y.; Chater, P. A.; Day, S. J.; Drakopoulos, M.; Gerring, M. W.; Hart, M. L.; Magdysyuk, O. V.; Michalik, S.; Smith, A.; Tang, C. C.; Terrill, N. J.; Wharmby, M. T.; Wilhelm, H. Processing Two-Dimensional X-Ray Diffraction and Small-Angle Scattering Data in DAWN 2. *J. Appl. Crystallogr.* **2017**, *50* (3), 959–966. https://doi.org/10.1107/S1600576717004708.

(40) Wright, A. J.; Narine, S. S.; Marangoni, A. G. Comparison of Experimental Techniques

886 Used in Lipid Crystallization Studies. *JAOCS, J. Am. Oil Chem. Soc.* **2000**, *77* (12), 1239–
887 1242. https://doi.org/10.1007/s11746-000-0194-2.

888 (41) Loisel, C.; Keller, G.; Lecq, G.; Bourgaux, C.; Ollivon, M. Phase Transitions and
889 Polymorphism of Cocoa Butter. *JAOCS, J. Am. Oil Chem. Soc.* **1998**, *75* (4), 425–439.
890 https://doi.org/10.1007/s11746-998-0245-y.

891 (42) Pérez-Martínez, D.; Alvarez-Salas, C.; Morales-Rueda, J. A.; Toro-Vazquez, J. F.; Charó-
892 Alonso, M.; Dibildox-Alvarado, E. The Effect of Supercooling on Crystallization of Cocoa
893 Butter-Vegetable Oil Blends. *JAOCS, J. Am. Oil Chem. Soc.* **2005**.
894 https://doi.org/10.1007/s11746-005-1096-z.

895 (43) Perez-Martınez, D.; Alvarez-Salas, C.; Charo-Alonso, M.; Dibildox-Alvarado; Toro-
896 Vazquez, J. . The Cooling Rate Effect on the Microstructure and Rheological Properties of
897 Blends of Cocoa Butter with Vegetable Oils. **2007**, *40*, 47–62.
898 https://doi.org/10.1016/j.foodres.2006.07.016.

899 (44) Acevedo, N. C.; Block, J. M.; Marangoni, A. G. Critical Laminar Shear-Temperature
900 Effects on the Nano- and Mesoscale Structure of a Model Fat and Its Relationship to Oil
901 Binding and Rheological Properties. *Faraday Discuss.* **2012**, *158*, 171–194.
902 https://doi.org/10.1039/c2fd20008b.

903 (45) Tran, T.; Ghosh, S.; Rousseau, D. Spheroidal Fat Crystal Microstructures Formed with
904 Confined Gap Shearing. *Cryst. Growth Des.* **2014**, *14* (12), 6383–6390.
905 https://doi.org/10.1021/cg501221d.

906 (46) Acevedo, N. C.; Marangoni, A. G. Characterization of the Nanoscale in Triacylglycerol

907 Crystal Networks. *Cryst. Growth Des.* **2010**, *10* (8), 3327–3333.
908 https://doi.org/10.1021/cg100468e.

909 (47) Bayés-García, L.; Calvet, T.; Cuevas-Diarte, M. À.; Ueno, S.; Sato, K. Heterogeneous
910 Microstructures of Spherulites of Lipid Mixtures Characterized with Synchrotron Radiation
911 Microbeam X-Ray Diffraction. *CrystEngComm* **2011**, *13* (22), 6694–6705.
912 https://doi.org/10.1039/c1ce05667k.

913 (48) Sato, K.; Bayés-García, L.; Calvet, T.; Cuevas-Diarte, M. À.; Ueno, S. External Factors
914 Affecting Polymorphic Crystallization of Lipids. *Eur. J. Lipid Sci. Technol.* **2013**, *115* (11),
915 1224–1238. https://doi.org/10.1002/ejlt.201300049.

916 (49) Tran, T.; Rousseau, D. Influence of Shear on Fat Crystallization. *Food Res. Int.* **2016**, *81*,
917 157–162. https://doi.org/10.1016/j.foodres.2015.12.022.

918 (50) Sonwai, S.; Mackley, M. R. The Effect of Shear on the Crystallization of Cocoa Butter.
919 *JAOCS, J. Am. Oil Chem. Soc.* **2006**, *83* (7), 583–596. https://doi.org/10.1007/s11746-006-
920 1243-6.

921 (51) Simone, E.; McVeigh, J.; Reis, N. M.; Nagy, Z. K. A High-Throughput Multi-Microfluidic
922 Crystal Generator (MMicroCryGen) Platform for Facile Screening of Polymorphism and
923 Crystal Morphology for Pharmaceutical Compounds. *Lab Chip* **2018**, *18* (15), 2235–2245.
924 https://doi.org/10.1039/c8lc00301g.

925 (52) Pérez-Martínez, J. D.; Reyes-Hernández, J.; Dibildox-Alvarado, E.; Toro-Vazquez, J. F.
926 Physical Properties of Cocoa Butter/Vegetable Oil Blends Crystallized in a Scraped Surface
927 Heat Exchanger. *JAOCS, J. Am. Oil Chem. Soc.* **2012**, *89* (2), 199–209.

https://doi.org/10.1007/s11746-011-1904-y.

(53) Gunes, D. Z.; Murith, M.; Godefroid, J.; Pelloux, C.; Deyber, H.; Schafer, O.; Breton, O. Oleofoams: Properties of Crystal-Coated Bubbles from Whipped Oleogels-Evidence for Pickering Stabilization. *Langmuir* **2017**, *33* (6), 1563–1575. https://doi.org/10.1021/acs.langmuir.6b04141.

(54) Fameau, A. L.; Saint-Jalmes, A. Non-Aqueous Foams: Current Understanding on the Formation and Stability Mechanisms. *Advances in Colloid and Interface Science*. 2017. https://doi.org/10.1016/j.cis.2017.02.007.

938